Measurement of the B_c^- meson production fraction and asymmetry in 7 and 13 TeV pp collisions

R. Aaij *et al.*[*]
(LHCb Collaboration)

(Received 30 October 2019; published 13 December 2019)

The production fraction of the B_c^- meson with respect to the sum of B^- and $\bar{B}^0$ mesons is measured in both 7 and 13 TeV center-of-mass (c.m.) energy pp collisions produced by the Large Hadron Collider (LHC), using the LHCb detector. The rate, approximately 3.7 per mille, does not change with energy, but shows a transverse momentum dependence. The $B_c^- - B_c^+$ production asymmetry is also measured and is consistent with zero within the determined statistical and systematic uncertainties of a few percent.

DOI: 10.1103/PhysRevD.100.112006

I. INTRODUCTION

The B_c^- meson is a bound state containing a b quark with a $\bar{c}$ quark.[1] It has the largest mass of any two differently flavored quarks in a mesonic ground state. Studies of its production or determination of individual decay widths require measurements of its branching fractions to exclusive final states. Since the branching fractions of some decay modes of B^- and $\bar{B}^0$ mesons are accurately known, we determine the ratio of B_c^- meson production relative to the sum of B^- and $\bar{B}^0$ mesons. Here we use techniques similar to those employed for the measurement of $\bar{B}_s^0$ meson and Λ_b^0 baryon fractions [1]. In that paper, use is made of the fact that the semileptonic widths of all b-flavored hadrons with light and strange quarks are equal. However, both the b and c quarks can decay, rendering that concept inapplicable. Instead, we rely on theoretical predictions of the semileptonic decay branching fraction $\mathcal{B}(B_c^- \to J/\psi\mu^-\bar{\nu})$. Currently, only the relative production cross-section times the branching fraction of either the $B_c^- \to J/\psi\mu^-\bar{\nu}$ or $B_c^- \to J/\psi\pi^-$ modes have been measured by the CDF [2,3], LHCb [4,5], and CMS [6,7] experiments.

The B_c^- meson production fraction (f_c) relative to the sum of $\bar{B}^0$ (f_d) and B^- (f_u) mesons is defined as

$$R_c = \frac{f_c}{f_u + f_d} \equiv \frac{n_{\rm cor}(B_c^- \to J/\psi\mu^-\bar{\nu})}{n_{\rm cor}(B \to D^0 X\mu^-\bar{\nu}) + n_{\rm cor}(B \to D^+ X\mu^-\bar{\nu})} \cdot \frac{\langle \mathcal{B}_{\rm sl} \rangle}{\mathcal{B}(B_c^- \to J/\psi\mu^-\bar{\nu})}, \quad (1)$$

where $n_{\rm cor}$ refers to the efficiency and $J/\psi, D$ branching fraction corrected number of signal events. The modes containing D^0 and D^+ mesons are also corrected for cross-feeds with $\bar{B}_s^0$ and Λ_b^0 decays. The determination of the corrected yields of the $B \to DX\mu^-\bar{\nu}$ decays follows our previous measurement strategy in Ref. [1] where the equations relating the fractions to the corrected yields, including cross-feed contributions, are given. We also correct for the 0.4% effect of doubly Cabibbo-suppressed decays and D^0 mixing. The relevant hadron branching fractions are listed in Table I. The average semileptonic branching fractions of $\bar{B}^0$ and B^-, $\langle \mathcal{B}_{\rm sl} \rangle = (10.70 \pm 0.19)\%$ is found by averaging measurements from the CLEO [8], *BABAR* [9], and Belle [10] experiments, detailed in Ref. [11]. Since only $b \to c\mu^-\bar{\nu}_\mu$ modes are detected in this analysis, a correction for the small $b \to u\mu^-\bar{\nu}_\mu$ rate of 1% is applied to the denominator of Eq. (1).

The dominant production mechanism for B_c^- mesons is gluon-gluon fusion, $gg \to B_c^- + \bar{b} + c$. Nonrelativistic quantum chromodynamics is used along with fragmentation functions to predict cross-sections as functions of transverse momentum ($p_{\rm T}$) and pseudorapidity (η). The literature is nicely summarized in Ref. [14]. We define H_b to refer to B_c, $\bar{B}^0$, and B^- mesons, while H_c refers to D^0 and D^+ mesons.

In this analysis, η is determined by measuring the angle of the B meson with respect to the beam direction by using the positions of the primary pp interaction vertex (PV) and

[*]Full author list given at the end of the article.

[1]The mention of a particular state implies the use of the charge-conjugate state as well, except when discussing production asymmetries.

TABLE I. Charm and charmonium branching fractions for the decay modes used in this analysis.

Particle and decay	$\mathcal{B}(\%)$	Source
$D^0 \to K^-\pi^+$	3.93 ± 0.05	PDG average [12]
$D^+ \to K^-\pi^+\pi^+$	9.22 ± 0.17	CLEO III [13]
$J/\psi \to \mu^+\mu^-$	5.96 ± 0.03	PDG average [12]

the B meson decay point into either $J/\psi\mu^-$, $D^0\mu^-$, or $D^+\mu^-$. The transverse momentum initially refers to the vector sum of the charmed-hadron and μ^- momentum transverse to the proton beams. However, the results are reinterpreted in terms of the H_b meson $p_{\rm T}(H_b)$ by simulating and correcting the effects of the missing momenta.

The production asymmetry between B_c^- and B_c^+ mesons, which should be small, is defined as

$$a_{\rm prod} \equiv \frac{\sigma(B_c^-) - \sigma(B_c^+)}{\sigma(B_c^-) + \sigma(B_c^+)} = a_{\rm raw} - a_{\rm det}, \qquad (2)$$

where the $a_{\rm raw}$ and $a_{\rm det}$ are the asymmetries in the signal yields and the efficiencies of B_c^- and B_c^+ detection, respectively. The CP asymmetry in the $B_c^- \to J/\psi\mu^-\bar{\nu}$ decay is assumed to be zero in this analysis.

The branching fraction predictions from various models of semileptonic B_c^- decays are listed in Table II. For $\mathcal{B}(B_c^- \to J/\psi\mu^-\bar{\nu})$, they range from 1.4% to 7.5%, which is quite a large interval. Branching fractions for other modes are also listed where available. We use the Z expansion fit results from Ref. [15] and the method II results for Ref. [16].

Some restrictions on models are possible by comparing to lighter B meson decays. Since the inclusive semileptonic branching fraction for these decays, $\mathcal{B}_{\rm sl}$, is about 10.5% and the B_c^- lifetime, τ_{B_c}, is 1/3 that of the $\bar{B}^0$, we disregard models that predict 10% or larger values for $\mathcal{B}_{\rm sl}^c$ of the B_c^-.[2] This excludes from consideration the models of Refs. [17] and [20]. The average model prediction then is $\mathcal{B}(B_c^- \to J/\psi\mu^-\bar{\nu}) = 1.95\%$. The standard deviation is 0.46%, which we use to estimate the systematic uncertainty on the model variation. Results of our measurement without using this branching fraction are also quoted.

TABLE II. Branching fractions predictions (%). The B_c^- lifetime is taken as 0.507 ps [12]. The value for the semileptonic decays of the B_c^- meson, $\mathcal{B}_{\rm sl}^c$, is derived by summing the $J/\psi\mu^-\bar{\nu}$ and $\eta_c\mu^-\bar{\nu}$ individual predictions with the average predictions of 0.1% for $\psi(2S)\mu^-\bar{\nu}$, the sum of $\chi_{c0,1,2}\mu^-\bar{\nu}$ as 0.6%, and 0.3% for $h_c\mu^-\nu$. In one case, where $\eta_c\mu^-\bar{\nu}$ was not predicted, averages from other measurements are used.

Ref.\Mode	$J/\psi\mu^-\bar{\nu}$	$\eta_c\mu^-\bar{\nu}$	$\psi(2S)\mu^-\bar{\nu}$	$\chi_{c0,1,2}\mu^-\bar{\nu}$	$h_c\mu^-\nu$	$\mathcal{B}_{\rm sl}^c$
[17]	6.4	5.0	1.3			13.6
[18]				0.5		
[19]	1.4	0.5				2.9
[20]	7.5	2.4				10.9
[21]	1.9	0.6	0.1			3.5
[22]	2.3	0.9		0.8		4.2
[23]	2.7	1.8				5.5
[24]	1.6	0.8				3.4
[25]	1.7	0.5		0.6		3.3
[26]	1.7	0.2				2.9
[27]	1.9	0.8	0.1			3.7
[28]	2.3	0.9				4.2
[29]	2.2	0.8	0.1			4.0
[30]	2.6		0.1	1.1		4.2
[31]	2.5	1.1				4.6
[32]	1.3	0.8	0.2			3.1
[33]	1.4	0.7				3.1
[15]	1.5	0.7		0.5	0.3	3.2
[16]	1.9	0.6	0.1	0.3	0.3	3.5
[34]	2.2	0.8				4.0

II. DETECTOR, TRIGGER, AND SIMULATION

The LHCb detector [35,36] is a single-arm forward spectrometer covering the pseudorapidity range $2 < \eta < 5$, designed for the study of particles containing b or c quarks. The detector elements that are particularly relevant to this analysis are a silicon-strip vertex detector surrounding the pp interaction region that allows c and b hadrons to be identified from their characteristically long flight distance; a tracking system that provides a measurement of the momentum, p, of charged particles; two ring-imaging Cherenkov detectors that are able to discriminate between different species of charged hadrons; and a downstream system of iron interspersed with chambers is used to identify muons.

The magnetic field deflects positively and negatively charged particles in opposite directions and this can lead to detection asymmetries. Periodically reversing the magnetic field polarity throughout the data taking almost cancels the effect. The configuration with the magnetic field pointing upward (downward) bends positively (negatively) charged particles in the horizontal plane toward the center of the LHC ring. This analysis uses data collected in 2011 (7 TeV) and 2016 (13 TeV) where appropriate triggers are available. The data taking was split between magnetic field up and down configurations. In the 2011 data, 0.6 fb^{-1} (0.4 fb^{-1}) was collected with the field pointing up (down), while in 2016 the split was 0.9 fb^{-1} with field up and 0.8 fb^{-1} with field down.

The trigger [37] consists of a hardware stage, based on information from the calorimeter and muon systems, followed by a software stage, in which all charged particles with $p_{\rm T} > 500(300)$ MeV are reconstructed for 2011 (2016) data.

[2]This is evident since $\mathcal{B}_{\rm sl}^c = \Gamma_{\rm sl} \cdot \tau_{B_c}$, and $\Gamma_{\rm sl}$ is approximately the same for all b-hadron species. We use natural units where $c = \hbar = 1$.

Separate hardware triggers are used for the $J/\psi\mu^-$ and H_c samples. For the former, we require a $\mu^+\mu^-$ pair. For the latter, we require a single muon with large p_T for the 7 TeV data as used in Ref. [38]. For the 13 TeV data, the single muon trigger was not available; therefore, at the hardware trigger stage, events are required to have a hadron, photon, or electron transverse energy greater than approximately 3.5 GeV in the calorimeters. The software trigger requires a two-, three-, or four-track secondary vertex with a significant displacement from any primary pp interaction vertex as described in Ref. [1]. At least, one charged particle must have $p_T > 1.6$ GeV and be inconsistent with originating from a PV. A multivariate algorithm [39] is used for the identification of secondary vertices consistent with the decay of a b hadron.

Simulation is required to model the effects of the detector acceptance and the imposed selection requirements. In the simulation, pp collisions are generated using PYTHIA [40] with a specific LHCb configuration [41]. Decays of unstable particles are described by EVTGEN [42], in which final-state radiation is generated using PHOTOS [43]. The interaction of the generated particles with the detector, and its response, are implemented using the GEANT4 toolkit [44], as described in Ref. [45].

III. EVENT SELECTION, SIGNAL EFFICIENCIES AND YIELDS

A. Selection of $B_c^- \to J/\psi\mu^-\bar{\nu}$ candidates

The analysis is done separately for the light B meson modes and the $B_c^- \to J/\psi\mu^-\bar{\nu}$ decay. In each case, the triggered events are subject to further filtering requirements. In addition, the $J/\psi\mu^-$ sample is subjected to a boosted decision tree (BDT), a multivariate classification method, using the TMVA toolkit [46]. This is not necessary for the D^0 or D^+ modes because they have large signals and are relatively free from backgrounds [1].

For the $J/\psi\mu^-\bar{\nu}$ final state, the initial selection requires that muons that satisfy the J/ψ candidate trigger each have minimum $p_T > 550$ MeV, have large impact parameters with the PV, form a good quality vertex, have a reasonable flight distance significance from the PV, and have a summed $p_T > 2$ GeV. The "companion" muon that is not part of the J/ψ decay must be well identified and form a good quality vertex with the J/ψ candidate, which must be downstream of the PV.

To suppress muon tracks that are reconstructed more than once, we require a small minimum opening angle between the muons from the J/ψ decay and the companion muon momentum measured in the plane transverse to the beam line. Specifically, this opening angle must be greater than 0.8°. The invariant mass of the companion muon and the oppositely charged muon from J/ψ must differ from the known value of the J/ψ mass by more than 50 MeV [12], while the invariant mass with the same charged muon is required to be larger than 400 MeV.

Since we are dealing with an exclusive final state, we define

$$m_{\rm cor} \equiv \sqrt{m(J/\psi\mu^-)^2 + p_\perp^2} + p_\perp, \tag{3}$$

where $p_\perp$ is the magnitude of the combination's momentum component transverse to the b-hadron flight direction. Figure 1 shows the distributions of $m_{\rm cor}$ versus the invariant $J/\psi\mu^-$ mass, $m(J/\psi\mu^-)$, for both data and simulation. To remove background, a requirement of $m(J/\psi\mu^-) > 4.5$ GeV is applied, as indicated by the (red) dashed line.

Since we also measure the production asymmetry between B_c^+ and B_c^- mesons, we restrict the angular acceptance of the companion muon to make it more uniform by removing muons close to the edge of the detector, in the bending direction (x-direction), where large acceptance-induced asymmetries can occur. Thus, we require that the x-component of the momentum satisfies

$$|p_x| \leq 0.294(p_z - 2\ \text{GeV}), \tag{4}$$

where p_z is the muon momentum along the direction of the proton beam downstream of the PV, as is done in Refs. [47,48].

After these initial restrictions, we turn to the multivariate selection, forming the classifier denoted BDT in the following. The discriminating variables used are (a) the χ^2 of the vertex fit of the J/ψ with the μ^-; (b) the $\ln\chi^2_{\rm IP}$, where $\chi^2_{\rm IP}$ is defined as the χ^2 of the impact parameter with respect to the PV, of the J/ψ, μ^-, and their combination; (c) the p_T of the J/ψ and the μ^-; and (d) the cosine of the angle between the μ^- and the J/ψ meson in the plane perpendicular to the beam direction. The training sample for signal is simulated $B_c^- \to J/\psi\mu^-\bar{\nu}$ events and for background is inclusive $b \to J/\psi X$ simulated events.

We then optimize the BDT output threshold by maximizing $S/\sqrt{S+B}$, where S and B are the number of the signal and background yields in the signal region defined as $m_{\rm cor} \in (4.8, 10.8)$ GeV. The sum, $S+B$, is the total number of events within these limits, and S is taken from a fit to the $m_{\rm cor}$ distribution. The optimal BDT output threshold results in a BDT signal efficiency of 89% with a background rejection of 63%, as determined by observing the resulting samples of input signal simulation events and background candidates.

The $m_{\rm cor}$ distribution is shown in Fig. 2. It consists not only of signal B_c^- events, but also of $B_c^- \to J/\psi\tau^-\bar{\nu}$ decays, where $\tau^- \to \mu^-\nu\bar{\nu}$, and other $c\bar{c}$ final states, most importantly $B_c^- \to \psi(2S)\mu^-\bar{\nu}$ and $B_c^- \to \chi_c\mu^-\bar{\nu}$. We find shapes for these final states using simulation. The signal shape is a sum of a double crystal ball and a bifurcated Gaussian function. The sum of the combinatorial and misidentification backgrounds is represented by a Gaussian kernel shape [49]. For the other background modes, we use histograms directly. These shapes are fitted to the $m_{\rm cor}$ distributions in Fig. 2 in order to determine the $B_c^- \to J/\psi\mu^-\bar{\nu}$ yields. The

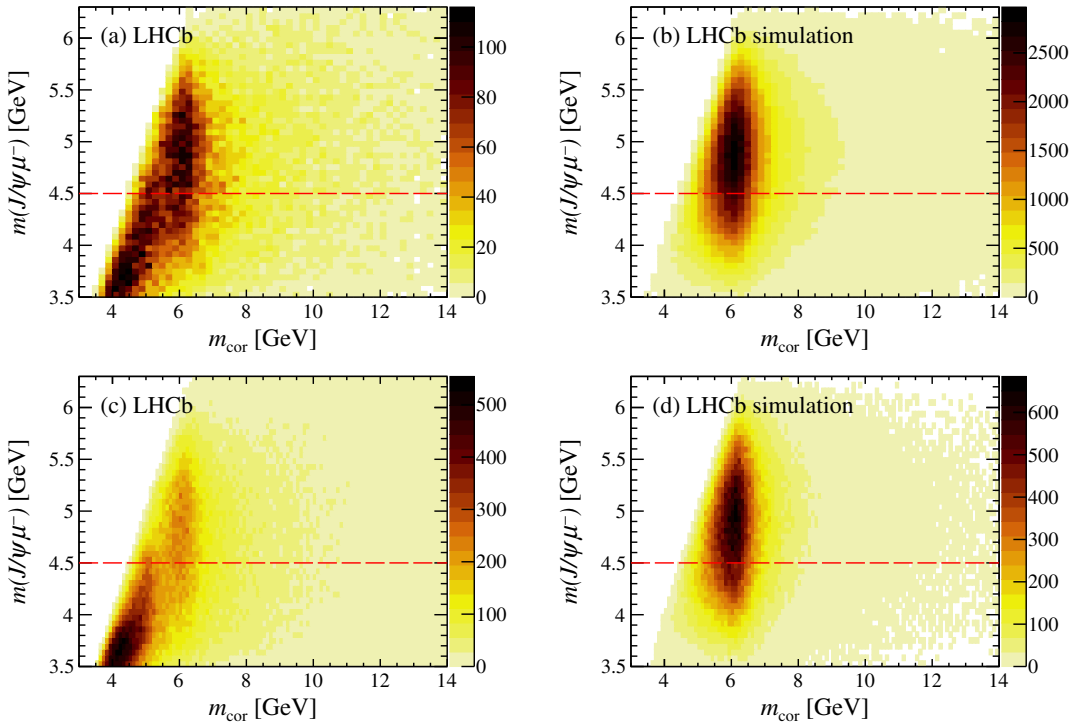

FIG. 1. Distributions of corrected mass $m_{\rm cor}$ and $m(J/\psi\mu^-)$ for (top) 7 TeV and (bottom) 13 TeV data, where (a) and (c) are data and (b) and (d) simulated signal. The (red) dashed line indicates the $m(J/\psi\mu^-) > 4.5$ GeV requirement.

ratio of the $J/\psi\tau^-\bar{\nu}$ yield to the $J/\psi\mu^-\bar{\nu}$ yield is fixed, after accounting for the relative detection efficiencies, from the LHCb measurement of $0.71 \pm 0.17 \pm 0.18$, where the first uncertainty is statistical and the second systematic [50]; this convention is used throughout this paper. The other components of the fit are allowed to vary. We find 4010 ± 200 and 15170 ± 710 signal $B_c^- \to J/\psi\mu^-\bar{\nu}$ events at 7 and 13 TeV, respectively, while the backgrounds sum to 950 and 5170 events at the same energies. These signal yields need to be corrected for the small background from candidates with a correctly reconstructed J/ψ meson that is paired with a hadron misidentified as a muon.

B. Efficiency for $B_c^- \to J/\psi\mu^-\bar{\nu}$

Efficiencies are determined using both data [51,52] and simulation of $B_c^- \to J/\psi\mu^-\bar{\nu}$, with the generated events weighted to match the $p_{\rm T}(H_b)$, and η distributions observed in data. In addition, we weight accordingly the $\chi^2_{\rm IP}$ distribution of the muon associated with the J/ψ. Weighting the simulation is important since the total efficiencies are functions of these variables. Efficiencies using data include trigger and muon identification. Efficiencies using simulation include detector acceptance, reconstruction and event selection, and removal of beam crossings with an excess number of hits in the detector.

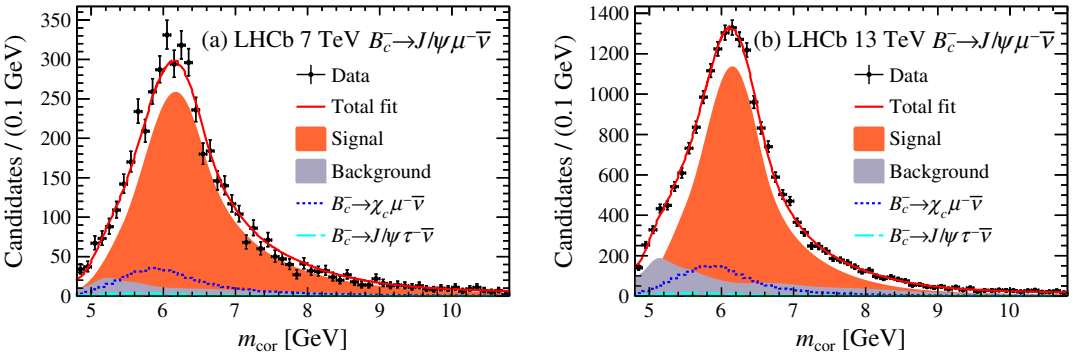

FIG. 2. Fitted $m_{\rm cor}$ distributions in (a) 7 TeV and (b) 13 TeV samples. The signal and the backgrounds are shown as the dark (orange) and lighter (gray) areas. The dashed (cyan) curves show the $B_c^- \to J/\psi\tau^-\nu_\tau$ components, while the dotted (blue) curves show the $B_c^- \to \chi_{c0,1,2}\mu^-\bar{\nu}$ components. The $B_c^- \to \psi(2S)\mu^-\bar{\nu}$ contribution is also in the fit but is too small to be seen. The total fit is shown by the solid (red) curve.

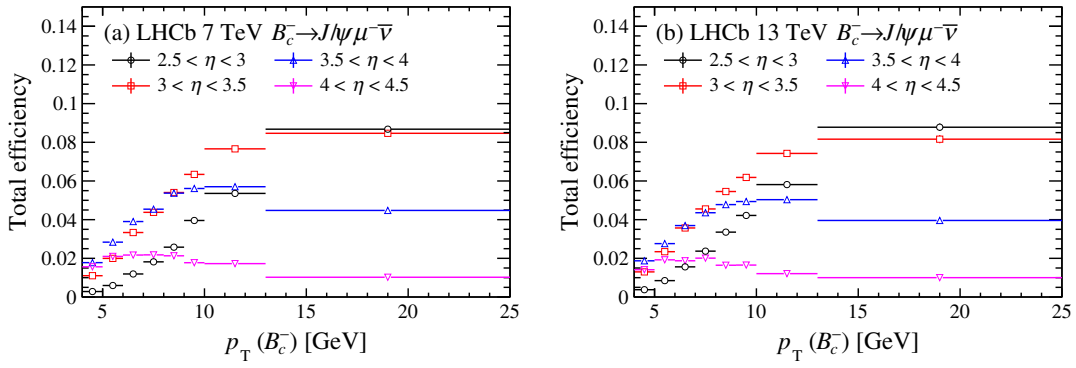

FIG. 3. The total efficiency for $B_c^- \to J/\psi\mu^-\bar{\nu}$, as a function of $p_T(B_c^-)$ in different intervals of η in (a) 7 TeV and (b) 13 TeV samples.

Total efficiencies as a function of $p_T(B_c^-)$ for different η intervals are shown in Fig. 3.

C. $H_cX\mu^-\bar{\nu}$ selection criteria

Selection criteria for $H_b \to H_cX\mu^-\bar{\nu}$ final states differ from those containing a J/ψ. The transverse momentum of each hadron must be greater than 0.3 GeV and that of the muon larger than 1.3 GeV. We require $\chi^2_{\rm IP} > 9$ with respect to any PV, ensuring that tracks do not originate from primary pp interactions. All final state particles are required to be positively identified using information from the RICH detectors. Particles from H_c decay candidates must have a good fit to a common vertex with $\chi^2/\text{n.d.o.f.} < 9$, where n.d.o.f. is the number of degrees of freedom. They must also be well separated from the nearest PV, with the flight distance divided by its uncertainty greater than five.

Candidate b hadrons are formed by combining H_c and muon candidates originating from a common vertex with $\chi^2/\text{n.d.o.f.} < 9$ and an $H_c\mu^-$ invariant mass in the range 3.0–5.0 GeV.

Background from prompt H_c production at the PV needs to be considered. We use the natural logarithm of the H_c impact parameter, IP, with respect to the PV in units of mm. Requiring $\ln(\text{IP/mm}) > -3$ is found to reduce the prompt component to be below 0.1%, while preserving 97% of all signals. This restriction allows us to perform fits only to the H_c candidate mass spectra to find the b-hadron decay yields.

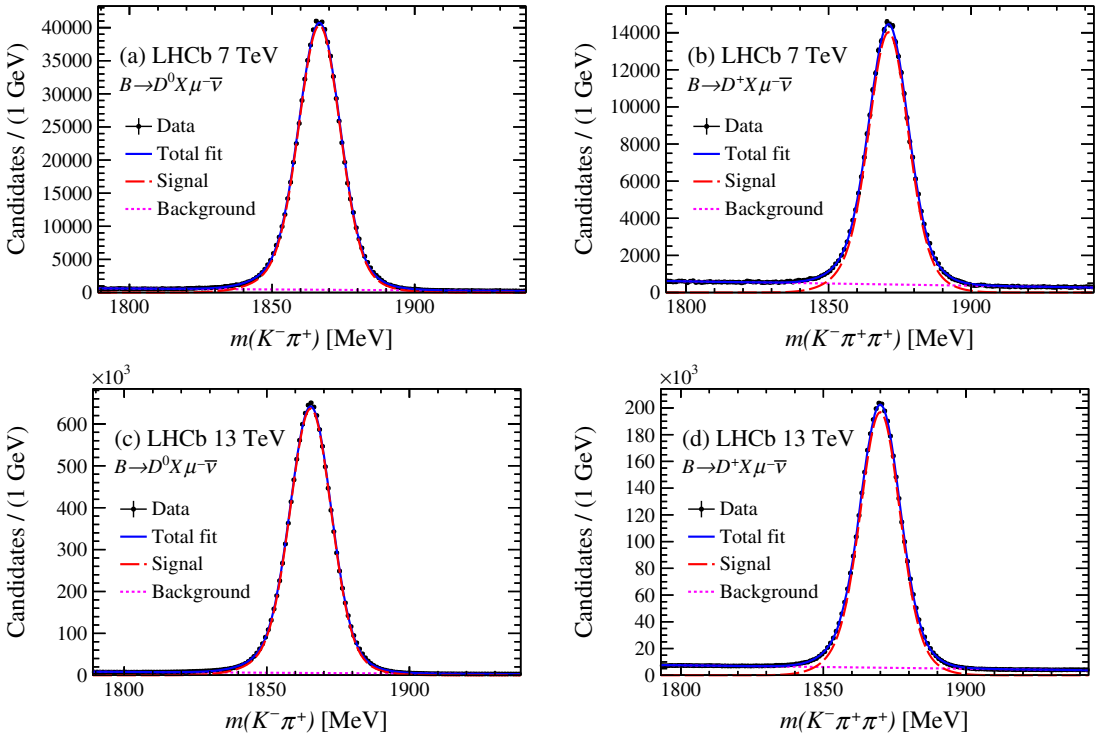

FIG. 4. Invariant-mass distributions of (a) $K^-\pi^+$ and (b) $K^-\pi^+\pi^+$ for 7 TeV, and (c) and (d) for 13 TeV collisions. The data are shown by solid points. The (red) dashed lines represent the signal components. The combinatorial backgrounds are shown as the dotted (magenta) line, and the solid (blue) line shows the total fit.

TABLE III. Yields of $B \to DX\mu^-\bar{\nu}$ decays.

	7 TeV yields		13 TeV yields	
Mode	Signal	Fake muons	Signal	Fake muons
$D^0X\mu\bar{\nu}$	789800 ± 940	5500 ± 160	12285000 ± 3700	115155 ± 580
$D^+X\mu\bar{\nu}$	263190 ± 570	990 ± 70	3686240 ± 2130	21370 ± 240

The H_c candidate mass distributions integrated over $p_T(H_b)$ and η are shown in Fig. 4 and consist of a prominent peak resulting from signal, and a small contribution due to combinatorial background from random combinations of particles that pass the selection. They are fit with a signal component comprising two Gaussian functions and a combinatorial background component modeled as a linear function. The fitted yields are listed in Table III. These numbers must be corrected for hadrons that are misidentified as muons, and for semileptonic decays of $\bar{B}_s^0$ and Λ_b^0 hadrons that produce D^0 and D^+ mesons.

In Table III, the column labeled "fake muons" shows the yields of wrong-sign $D^0X\mu^+$ and $D^+X\mu^+$ combinations that pass the selections. These yields provide good estimates of the fake muon contributions in the signal samples, which are very small. Following the procedure in Ref. [1], we find the cross-feed corrections of $\bar{B}_s^0 \to (D^0 + D^+)X\mu^-\bar{\nu}$ and $\Lambda_b^0 \to (D^0 + D^+)X\mu^-\bar{\nu}$ to be twice the measured yields for $\bar{B}_s^0 \to D^0K^+X\mu^-\bar{\nu}$, which are 8500 ± 340 (7 TeV) and 69390 ± 1130 (13 TeV), and for $\Lambda_b^0 \to D^0pX\mu^-\bar{\nu}$, which are 2330 ± 140 (7 TeV) and 33050 ± 460 (13 TeV). Relative efficiencies for detecting final states with a single extra hadron are taken into account when subtracting these yields.

D. Efficiencies for $B \to D^0X\mu^-\bar{\nu}$ and $B \to D^+X\mu^-\bar{\nu}$

Similar methods based on data, as implemented for the B_c^- decay, are used to evaluate the efficiencies for trigger and particle identification. Simulation is also used to determine the efficiencies of event selection and reconstruction of these modes. The total efficiencies for B meson decays into $D^0X\mu^-\bar{\nu}$ and $D^+X\mu^-\bar{\nu}$ are shown in Fig. 5.

IV. RESULTS

A. Corrections to the $p_T(H_b)$ distributions due to the missing neutrino

Since the production kinematics of B and B_c^- mesons can differ as functions of $p_T(H_b)$ and η, we need to measure $f_c/(f_u + f_d)$ as functions of these variables. The measurement of η is straightforward; however, we do not measure directly the $p_T(H_b)$ of the b-flavored hadron because of the missing neutrino, and in the case of the B meson possible missing extra particles. Following a procedure similar to the one used in Ref. [1], we determine a correction factor, k, that is the ratio of the average reconstructed to true $p_T(H_b)$ as a function of the invariant mass of the charmed hadron plus muon. The ratio distribution as a function of hadron-muon invariant mass is shown in Fig. 6. The average correction, the k-factor, is shown in the figure. For the B meson, it varies from 0.75 to unity over the interval from 3 GeV to the B mass, and for the B_c^- meson, it varies from 0.85 to unity over the interval from 4 GeV to the B_c^- mass.

B. B_c^- fraction results

The ratio of production fractions, $f_c/(f_u + f_d)$, is shown as functions of $p_T(H_b)$ and η in Fig. 7. There is little dependence on η, but the decrease as a function of $p_T(H_b)$ is noticeable.

To describe the $p_T(H_b)$ dependence, we use an equation of the form

$$\frac{f_c}{f_u + f_d}(p_T) = A[p_1 + p_2(p_T(H_b) - \langle p_T \rangle)], \quad (5)$$

where A represents the overall normalization and contains the total global systematic uncertainty; thus, $A = 1 \pm 0.24$;[3] $\langle p_T \rangle$ is taken as 7.2 GeV, close to the average p_T of the B_c^-. The slopes, p_2, are similar in size to those measured for the B_s meson fraction ratio as a function of p_T [1,53]. Results of fits to the data using Eq. (5) are listed in Table IV.

The average fractions in the interval $4 < p_T(H_b) < 25$ GeV are found by integrating over $p_T(H_b)$. To allow for facile changes to our results due to improved theoretical predictions, we provide the results for

$$\frac{f_c}{f_u + f_d} \cdot \mathcal{B}(B_c^- \to J/\psi\mu^-\bar{\nu}) = (7.07 \pm 0.15 \pm 0.24) \times 10^{-5} \quad \text{for 7 TeV},$$

$$\frac{f_c}{f_u + f_d} \cdot \mathcal{B}(B_c^- \to J/\psi\mu^-\bar{\nu}) = (7.36 \pm 0.08 \pm 0.30) \times 10^{-5} \quad \text{for 13 TeV}.$$

[3]See Sec. V for the discussion of the systematic uncertainties.

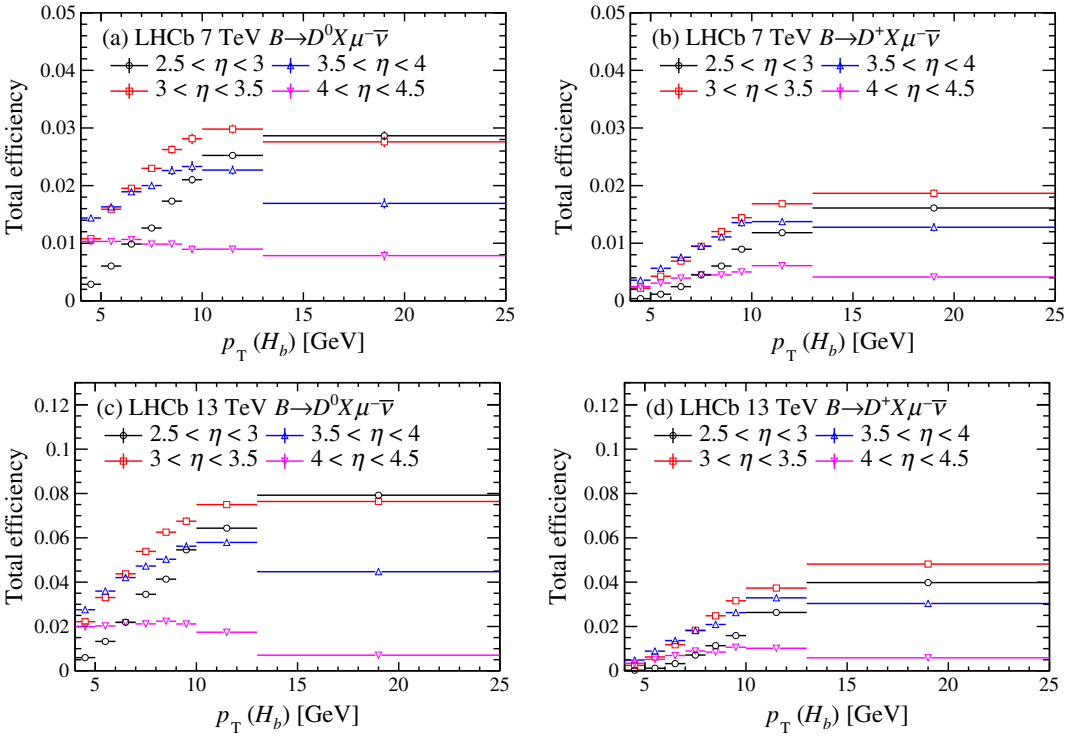

FIG. 5. Total efficiencies for the (a) $D^0X\mu^-\bar{\nu}$ and (b) $D^+X\mu^-\bar{\nu}$ signals in 7 TeV and (c) and (d) 13 TeV samples as functions of p_T in η intervals.

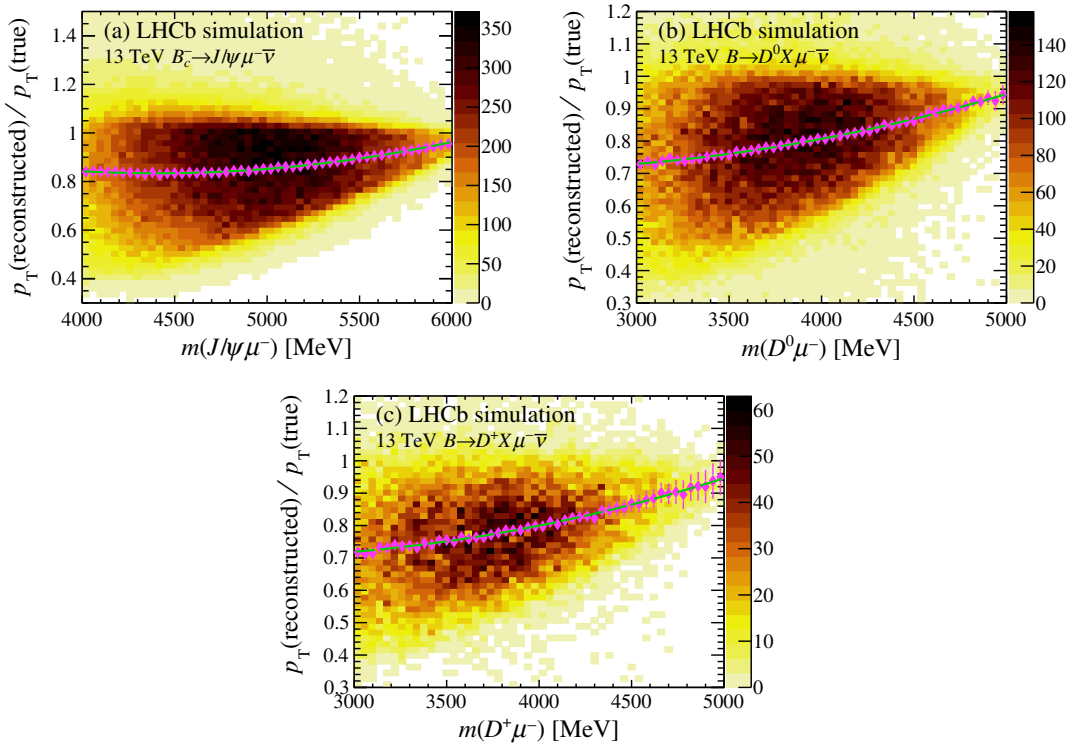

FIG. 6. The k-factor corrections as a function of invariant mass of (a) $m(J/\psi\mu^-)$, (b) $m(D^0\mu^-)$, and (c) $m(D^+\mu^-)$ for the 13 TeV simulation samples. (The 7 TeV results are almost identical.) The points (magenta) are the average k-factor corrections, and the (green) dashed line shows a second-order polynomial fit to the average data.

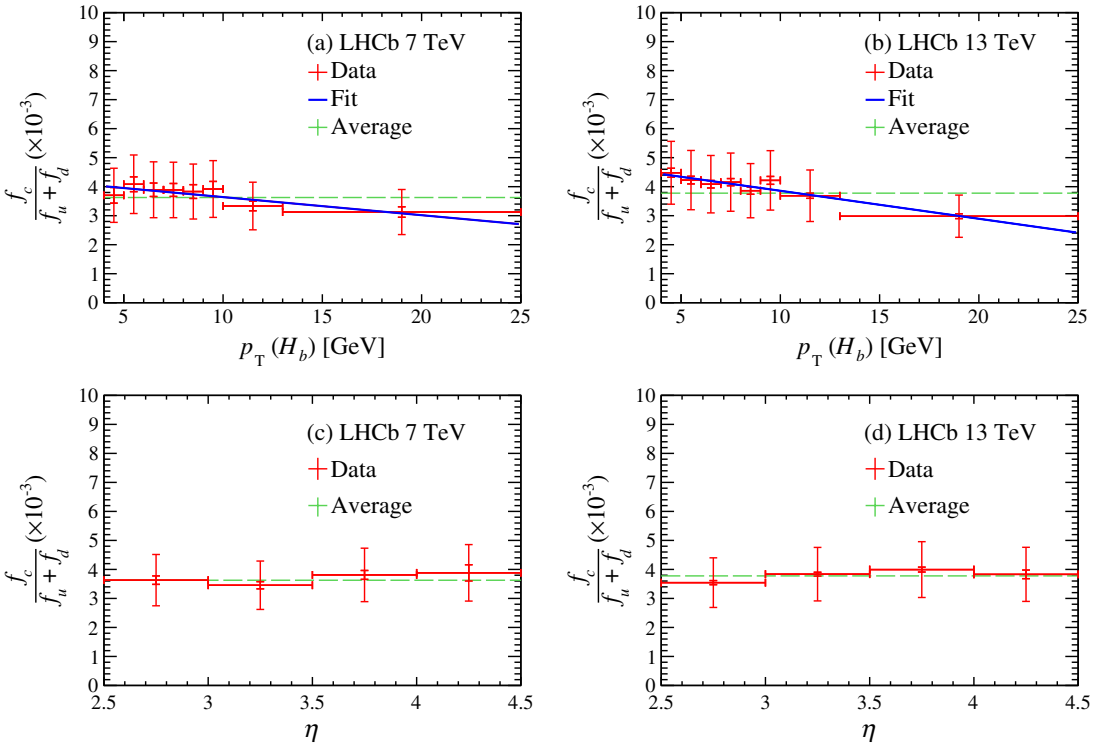

FIG. 7. Ratio of production fractions after the k-factor correction as a function of (a) $p_T(H_b)$ and (c) η in 7 TeV data and (b) and (d) in 13 TeV data. The smaller error bars show the statistical uncertainties, and the larger ones include the statistical and systematic uncertainties. The horizontal (green) dashed-lines show the average values.

Next, we give the result on the fractions ratio

$$\frac{f_c}{f_u+f_d} = (3.63 \pm 0.08 \pm 0.12 \pm 0.86) \times 10^{-3} \quad \text{for 7 TeV},$$
$$\frac{f_c}{f_u+f_d} = (3.78 \pm 0.04 \pm 0.15 \pm 0.89) \times 10^{-3} \quad \text{for 13 TeV},$$

where the third uncertainty is due to the theoretical prediction of $\mathcal{B}(B_c^- \to J/\psi\mu^-\bar{\nu})$. To find f_c/f_u, just double these numbers.

We also measure the ratio of the B_c^- production fraction at 7 TeV to that at 13 TeV. Figure 8 shows the ratio as functions of p_T and η. Here most of the systematic uncertainties cancel. The integrated value of the ratio of 13 and 7 TeV is measured as $1.02 \pm 0.02 \pm 0.04$, consistent with no increase in the B_c^- fraction ratio as a function of c.m. energy.

The B_c^- fraction with respect to inclusive b-hadron production can be derived from the information in previous LHCb b-hadron fraction papers in Ref. [1,38,53]. There the measured values of the ratios of b-hadron fractions over the same p_T range in terms of the b-hadron p_T are for $\bar{B}_s^0$ mesons (f_s) and Λ_b^0 baryons,

$$\frac{f_s}{f_u+f_d} = \begin{cases} 0.124 \pm 0.010 & (7\text{ TeV})\,[53] \\ 0.122 \pm 0.006 & (13\text{ TeV})\,[1], \end{cases} \tag{6}$$

$$\frac{f_{\Lambda_b^0}}{f_u+f_d} = \begin{cases} 0.223 \pm 0.036 & (7\text{ TeV})\,[38] \\ 0.259 \pm 0.018 & (13\text{ TeV})\,[1], \end{cases} \tag{7}$$

where the uncertainties contain both statistical and systematic components added in quadrature. For the measurement of the $f_{\Lambda_b^0}$ fraction at 7 TeV, the dominant systematic uncertainty is from the lack of the knowledge of $\mathcal{B}(\Lambda_c^+ \to pK^-\pi^+)$ at that time [38]; here the value and uncertainty have been recalculated according to the latest value of $\mathcal{B}(\Lambda_c^+ \to pK^-\pi^+)$ from the PDG [12].

Taking the sum of all the b-hadron fractions to be unity, and ignoring f_c here because it is so small,

$$f_u + f_d + f_s + f_{\Lambda_b^0}(1+\delta) = 1, \tag{8}$$

where $\delta = 0.25 \pm 0.10$ is a correction factor derived in Ref. [11] that accounts for heavier b-baryons, mainly the Ξ_b. Solving for $f_u + f_d$ yields

TABLE IV. Results of the fits to Eq. (5).

Energy	p_1	$p_2 \times 10^{-2}$ (GeV^{-1})
7 TeV	$3.82 \pm 0.09 \pm 0.05$	$-6.2 \pm 1.7 \pm 1.1$
13 TeV	$4.13 \pm 0.05 \pm 0.04$	$-9.7 \pm 0.8 \pm 1.0$

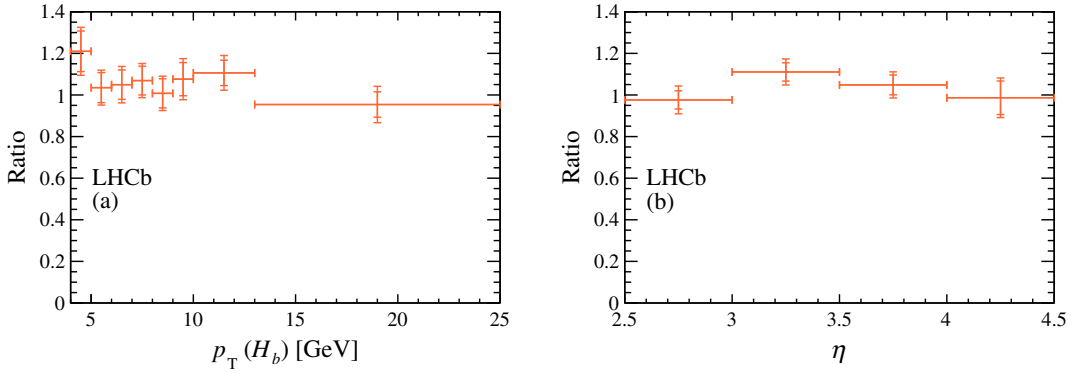

FIG. 8. Ratio of the B_c^- production fractions at 13–7 TeV as a function of (a) $p_T(H_b)$ and (b) η. The smaller error bars show the statistical uncertainties, and the larger ones include the statistical and systematic uncertainties added in quadrature.

$$f_u + f_d = \left(1 + \frac{f_s}{f_u + f_d} + \frac{f_{\Lambda_b^0}}{f_u + f_d}(1+\delta)\right)^{-1}, \\ = \begin{cases} 0.713 \pm 0.026 & (7\ \text{TeV}) \\ 0.692 \pm 0.015 & (13\ \text{TeV}). \end{cases} \tag{9}$$

We find that

$$f_c \cdot \mathcal{B}(B_c^- \to J/\psi\mu^-\bar{\nu}) = \begin{cases} (5.04 \pm 0.11 \pm 0.17 \pm 0.18) \times 10^{-5} & (7\ \text{TeV}) \\ (5.09 \pm 0.06 \pm 0.21 \pm 0.11) \times 10^{-5} & (13\ \text{TeV}) \end{cases},$$

where the first uncertainty is statistical, the second is systematic, and the third is from the fractions of the B_s^0 and Λ_b^0 given in Eq. (9). We also provide the result for f_c,

$$f_c = \begin{cases} (2.58 \pm 0.05 \pm 0.62 \pm 0.09) \times 10^{-3} & (7\ \text{TeV}) \\ (2.61 \pm 0.03 \pm 0.62 \pm 0.06) \times 10^{-3} & (13\ \text{TeV}) \end{cases},$$

where the first uncertainty is statistical, the second is systematic including that from $\mathcal{B}(B_c^- \to J/\psi\mu^-\bar{\nu})$, and the third is from the fractions of the B_s^0 and Λ_b^0 given in Eq. (9).

C. The $B_c^- - B_c^+$ production asymmetry

The production asymmetries are measured in two different magnetic field configurations and then averaged. No significant asymmetry is observed in any intervals of $p_T(H_b)$ or η. The results are summarized in Table V.

Averaging the $B_c^- - B_c^+$ production asymmetries over $p_T(H_b)$ and η, we find $(-2.5 \pm 2.1 \pm 0.5)\%$ and $(-0.5 \pm 1.1 \pm 0.4)\%$ at c.m. energies of 7 and 13 TeV, respectively.

V. SYSTEMATIC UNCERTAINTIES

Systematic uncertainties are separated into two categories: "global," which applies across the phase space, and "local," which is calculated in each two-dimensional $p_T(H_b) - \eta$ bin. These uncertainties are listed in Table VI.

First, let us consider the $B_c^- \to J/\psi\mu^-\bar{\nu}$ decay. The uncertainty due to the signal shape used to fit the m_{cor} distribution is determined by changing the baseline signal

TABLE V. The $B_c^- - B_c^+$ production asymmetry ($\times 10^{-2}$) as a function of $p_T(H_b)$ and η at 7 and 13 TeV.

7 TeV production asymmetry		
p_T(GeV)\η	2.5–3.5	3.5–4.5
4–6	$7.91 \pm 7.00 \pm 1.03$	$-6.44 \pm 6.44 \pm 2.10$
6–8	$-4.34 \pm 5.43 \pm 1.62$	$-6.66 \pm 6.65 \pm 2.03$
8–10	$-1.13 \pm 6.31 \pm 1.56$	$-9.63 \pm 7.23 \pm 0.81$
10–25	$0.24 \pm 4.13 \pm 0.98$	$-4.87 \pm 8.63 \pm 1.44$
13 TeV production asymmetry		
p_T(GeV)\η	2.5–3.5	3.5–4.5
4–6	$3.13 \pm 3.33 \pm 1.16$	$1.76 \pm 3.23 \pm 0.91$
6–8	$-0.34 \pm 2.79 \pm 1.26$	$-5.03 \pm 3.61 \pm 1.06$
8–10	$2.03 \pm 2.73 \pm 0.94$	$-2.48 \pm 4.29 \pm 1.78$
10–25	$1.50 \pm 2.05 \pm 0.73$	$-1.47 \pm 4.20 \pm 2.18$

TABLE VI. Summary of the relative systematic uncertainties for $f_c/(f_u+f_d)(\%)$ and the absolute production asymmetries $a_{\rm prod}(\%)$. For local uncertainties, the ranges correspond to the minimum and maximum uncertainties evaluated in the $p_{\rm T}(H_b)$ and η ranges.

	$f_c/(f_u+f_d)$		$a_{\rm prod}$	
	7 TeV	13 TeV	7 TeV	13 TeV
Local uncertainties				
Signal shape	0.12–9.56	0.14–2.80	0.04–1.80	0.01–0.78
Background shape	0.34–6.16	0.02–5.80	0.06–3.05	0.05–2.45
Feed-down channels	0.12–5.00	0.43–2.27	0.01–1.11	0.03–0.65
Decay models	0.00–2.00	0.01–3.84	0.02–0.28	0.02–0.61
Muon ID in $J/\psi\mu^-$	0.06–5.79	0.03–2.92	0.02–0.37	0.01–0.18
Trigger for J/ψ	0.00–0.23	0.00–0.34	0.05–2.34	0.07–4.24
Simulation decay model	0.00–2.00	0.01–3.84	0.02–0.28	0.02–0.61
Hadron ID in $DX\mu^-\bar{\nu}$	0.04–1.81	0.01–2.01	⋯	⋯
Muon trigger & ID in $DX\mu^-\bar{\nu}$	0.02–1.34	0.00–0.21	⋯	⋯
Simulation sample size	1.5–11.5	2.1–10.7	0.5–1.1	0.5–1.2
k-factor	0.02–0.95	0.05–0.70	0.01–0.10	0.00–0.10
Tracking asymmetry	⋯	⋯	0.00–0.28	0.00–0.09
Global uncertainties				
$\mathcal{B}(J/\psi\to\mu^+\mu^-)$	0.55	0.55	⋯	⋯
$\mathcal{B}(D^+\to K^-\pi^+\pi^+)$ or $\mathcal{B}(D^0\to K^-\pi^+)$	1.0	1.0	⋯	⋯
$\mathcal{B}(B\to H_cX\mu^-\bar{\nu})$	1.8	1.8	⋯	⋯
Cross-feed contribution	0.2	0.2	⋯	⋯
Multiplicity cut	1.2	2.7	⋯	⋯
Tracking efficiency	1.8	1.8	⋯	⋯
Uncertainty sum	4.3–21.3	5.1–17.4	1.0–3.5	1.0–4.8
$\mathcal{B}(B_c^-\to J/\psi\mu^-\bar{\nu})$	23.6	23.6	⋯	⋯
Overall uncertainty	24.0–31.8	24.1–29.3	1.0–3.5	1.0–4.8

shape, the sum of a double sided crystal ball function and a bifurcated Gaussian, to a kernel estimation. To find the shape of the combinatorial and misidentification backgrounds, we use simulated inclusive samples of $b\to J/\psi X$ events not including B_c^- decays. A total of 500 samples are generated and different fits to the samples are performed to determine the possible uncertainty. This procedure is also used for the $a_{\rm prod}$ measurement. We call contributions to the $J/\psi\mu^-$ mass spectrum "feed-down" contributions, occurring from other B_c^- decay channels including $J/\psi\tau\bar{\nu}$, $\psi(2S)\mu^-\bar{\nu}$, and $\chi_c\mu^-\bar{\nu}$. The systematic uncertainty results from the uncertainties in their branching fractions. Different decay models for $B_c^-\to J/\psi\mu^-\bar{\nu}$ decays can change the $m_{\rm cor}$ shape. We use the model of Ebert *et al.* [18] for our baseline prediction. Then we also use the model by Kiselev [29] to find the efficiencies and take half the difference as the systematic uncertainty. We also estimate the uncertainty due to the sensitivity to various selection requirements and simulation statistics. The muon identification efficiencies are determined from data using inclusive samples of J/ψ decay where one of the muon candidates is not identified. The trigger efficiency is determined by using three independent samples of events, those that trigger on a J/ψ, those that triggered on something else in the event, and those that trigger on both the J/ψ and something else. These samples are then used to compute the trigger efficiencies in two-dimensional $p_{\rm T}(H_b)$ and η bins.

Next, we turn to the $B\to DX\mu\nu$ modes. The efficiencies and their uncertainties for identifying pions and kaons are determined by using almost background free samples of $D^{*+}\to\pi^+D^0$, $D^0\to K^-\pi^+$ decays. The trigger and muon identification efficiencies, and their uncertainties, are obtained in the same manner as for the $B_c^-\to J/\psi\mu^-\bar{\nu}$ mode. There are small systematic uncertainties related to efficiency estimates and the assumed D^* to D mixtures, as well as simulation statistics. Global systematic uncertainties include the hadron branching fractions listed in Table I, cross-feed corrections arising from $\bar{B}_s^0$ and Λ_b^0 decays into $DX\mu^-\bar{\nu}$ events, and a global hadron plus photon multiplicity requirement. The latter is evaluated with data.

VI. CONCLUSIONS

In 7 and 13 TeV pp collisions the product of $\mathcal{B}(B_c^-\to J/\psi\mu^-\bar{\nu})$ with the relative fraction of B_c^- mesons with respect to the sum of B^0 and B^+ mesons in the ranges $2.5<\eta<4.5$ and $4<p_{\rm T}(H_b),<25$ GeV is found to be

$$\frac{f_c}{f_u+f_d}\cdot\mathcal{B}(B_c^-\to J/\psi\mu^-\bar{\nu}) = (7.07\pm0.15\pm0.24)\times10^{-5} \quad \text{for 7 TeV},$$
$$\frac{f_c}{f_u+f_d}\cdot\mathcal{B}(B_c^-\to J/\psi\mu^-\bar{\nu}) = (7.36\pm0.08\pm0.30)\times10^{-5} \quad \text{for 13 TeV}.$$

We derive the product of $f_c\cdot\mathcal{B}(B_c^-\to J/\psi\mu^-\bar{\nu})$ at the two energies as

$$f_c\cdot\mathcal{B}(B_c^-\to J/\psi\mu^-\bar{\nu}) = \begin{cases}(5.04\pm0.11\pm0.17\pm0.18)\times10^{-5} & (7\text{ TeV})\\ (5.09\pm0.06\pm0.21\pm0.11)\times10^{-5} & (13\text{ TeV}).\end{cases}$$

Using the average of the theoretical prediction $\mathcal{B}(B_c^-\to J/\psi\mu^-\bar{\nu}) = (1.95\pm0.46)\%$, where the uncertainty is given by the standard deviation derived from the distribution of the models, we determine

$$\frac{f_c}{f_u+f_d} = (3.63\pm0.08\pm0.12\pm0.86)\times10^{-3} \quad \text{for 7 TeV},$$
$$\frac{f_c}{f_u+f_d} = (3.78\pm0.04\pm0.15\pm0.89)\times10^{-3} \quad \text{for 13 TeV},$$

where the first uncertainties are statistical, the second systematic, and the third due to the theoretical prediction of $\mathcal{B}(B_c^-\to J/\psi\mu^-\bar{\nu})$. There is a small dependence on the transverse momentum of the B_c^+ meson, but no dependence on its pseudorapidity is observed. We also report

$$f_c = \begin{cases}(2.58\pm0.05\pm0.62\pm0.09)\times10^{-3} & (7\text{ TeV})\\ (2.61\pm0.03\pm0.62\pm0.06)\times10^{-3} & (13\text{ TeV})\end{cases},$$

where the first uncertainty is statistical, the second is systematic including that from $\mathcal{B}(B_c^-\to J/\psi\mu^-\bar{\nu})$, and the third is from the fractions of the B_s^0 and Λ_b^0 given in Eq. (9).

The ratio of fractions, $1.02\pm0.02\pm0.04$, for 13 TeV/7 TeV is consistent with no increase in the B_c^- fraction. Furthermore, using the assumption of no CP violation in the $B_c^-\to J/\psi\mu^-\bar{\nu}$ decay, we find that the average asymmetry in $B_c^- - B_c^+$ production is consistent with zero. The measurements are $(-2.5\pm2.1\pm0.5)\%$ and $(-0.5\pm1.1\pm0.4)\%$ at c.m. energies of 7 and 13 TeV, respectively.

These results are useful to extract absolute branching fractions for B_c^- measurements, albeit with a relatively large uncertainty. They also challenge QCD calculations to predict the measured B_c^- fractions and explain the consistency between the fractions measured at 7 and 13 TeV [14,54].

ACKNOWLEDGMENTS

We express our gratitude to our colleagues in the CERN accelerator departments for the excellent performance of the LHC. We thank the technical and administrative staff at the LHCb institutes. We acknowledge support from CERN and from the national agencies: CAPES, CNPq, FAPERJ, and FINEP (Brazil); MOST and NSFC (China); CNRS/IN2P3 (France); BMBF, DFG, and MPG (Germany); INFN (Italy); NWO (Netherlands); MNiSW and NCN (Poland); MEN/IFA (Romania); MSHE (Russia); MinECo (Spain); SNSF and SER (Switzerland); NASU (Ukraine); STFC (United Kingdom); DOE NP and NSF (the United States). We acknowledge the computing resources that are provided by CERN, IN2P3 (France), KIT and DESY (Germany), INFN (Italy), SURF (Netherlands), PIC (Spain), GridPP (United Kingdom), RRCKI and Yandex LLC (Russia), CSCS (Switzerland), IFIN-HH (Romania), CBPF (Brazil), PL-GRID (Poland), and OSC (the United States). We are indebted to the communities behind the multiple open-source software packages on which we depend. Individual groups or members have received support from AvH Foundation (Germany); EPLANET, Marie Skłodowska-Curie Actions, and ERC (European Union); ANR, Labex P2IO and OCEVU, and Région Auvergne-Rhône-Alpes (France); Key Research Program of Frontier Sciences of CAS, CAS PIFI, and the Thousand Talents Program (China); RFBR, RSF, and Yandex LLC (Russia); GVA, XuntaGal, and GENCAT (Spain); the Royal Society and the Leverhulme Trust (United Kingdom).

[1] R. Aaij *et al.* (LHCb Collaboration), Measurement of b hadron fractions in 13 TeV pp collisions, Phys. Rev. D **100**, 031102 (2019).

[2] F. Abe *et al.* (CDF Collaboration), Observation of the B_c Meson in $p\bar{p}$ Collisions at $\sqrt{s} = 1.8$ TeV, Phys. Rev. Lett. **81**, 2432 (1998).

[3] F. Abe *et al.* (CDF Collaboration), Observation of B_c mesons in $p\bar{p}$ collisions at $\sqrt{s} = 1.8$ TeV, Phys. Rev. D **58**, 112004 (1998).

[4] R. Aaij *et al.* (LHCb Collaboration), Measurements of B_c^+ Production and Mass with the $B_c^+ \to J/\psi\pi^+$ Decay, Phys. Rev. Lett. **109**, 232001 (2012).

[5] R. Aaij *et al.* (LHCb Collaboration), Measurement of B_c^+ Production in Proton-Proton Collisions at $\sqrt{s} = 8$ TeV, Phys. Rev. Lett. **114**, 132001 (2015).

[6] CMS Collaboration, Measurement of $\frac{\sigma(B_c^+)\times\mathcal{B}(B_c^+\to J/\psi\pi^+)}{\sigma(B^+)\times\mathcal{B}(B^+\to J/\psi K^+)}$ and $\frac{\sigma(B_c^+)\times\mathcal{B}(B_c^+\to J/\psi\pi^+\pi^+\pi^-)}{\sigma(B_c^+)\times\mathcal{B}(B^+\to J/\psi\pi^+)}$ at $\sqrt{s} = 7$ TeV, CERN Report No. CMS-PAS-BPH-12-011, 2013.

[7] CMS Collaboration, Measurement of production cross sections times branching fraction of $B_c^+ \to J/\psi\pi^+$ and $B^+ \to J/\psi K^+$ in pp collisions at $\sqrt{s} = 7$ TeV at CMS, CERN Report No. CMS-PAS-BPH-13-002, 2018.

[8] A. H. Mahmood *et al.* (CLEO Collaboration), Measurement of the B-meson inclusive semileptonic branching fraction and electron energy moments, Phys. Rev. D **70**, 032003 (2004).

[9] B. Aubert *et al.* (*BABAR* Collaboration), Measurement of the ratio $\mathcal{B}(B^+ \to Xe\nu)/\mathcal{B}(B^0 \to Xe\nu)$, Phys. Rev. D **74**, 091105 (2006).

[10] P. Urquijo *et al.* (Belle Collaboration), Moments of the electron energy spectrum and partial branching fraction of $B \to X_c e\nu$ decays at Belle, Phys. Rev. D **75**, 032001 (2007).

[11] R. Aaij *et al.* (LHCb Collaboration), Measurement of the b-Quark Production Cross-Section in 7 and 13 TeV pp Collisions, Phys. Rev. Lett. **118** (2017) 052002; Erratum, Phys. Rev. Lett. **119**, 169901 (2017).

[12] M. Tanabashi *et al.* (Particle Data Group), Review of particle physics, Phys. Rev. D **98**, 030001 (2018).

[13] G. Bonvicini *et al.* (CLEO Collaboration), Updated measurements of absolute D^+ and D^0 hadronic branching fractions and $\sigma(e^+e^- \to D\bar{D})$ at $E_{\rm cm} = 3774$ MeV, Phys. Rev. D **89**, 072002 (2014); Erratum, Phys. Rev. D **91**, 019903 (2015).

[14] N. Brambilla *et al.*, Heavy quarkonium: Progress, puzzles, and opportunities, Eur. Phys. J. C **71**, 1534 (2011).

[15] W. Wang and R. Zhu, Model independent investigation of the $R_{J/\psi,\eta_c}$ and ratios of decay widths of semileptonic B_c decays into a P-wave charmonium, arXiv:1808.10830.

[16] Z.-K. Geng, T. Wang, Y. Jiang, G. Li, X.-Z. Tan, and G.-L. Wang, Relativistic effects in the semileptonic B_c decays to charmonium with the Bethe-Salpeter method, Phys. Rev. D **99**, 013006 (2019).

[17] Z. Rui, H. Li, G.-x. Wang, and Y. Xiao, Semileptonic decays of B_c meson to S-wave charmonium states in the perturbative QCD approach, Eur. Phys. J. C **76**, 564 (2016).

[18] D. Ebert, R. N. Faustov, and V. O. Galkin, Semileptonic and nonleptonic decays of B_c mesons to orbitally excited heavy mesons in the relativistic quark odel, Phys. Rev. D **82**, 034019 (2010).

[19] D. Ebert, R. N. Faustov, and V. O. Galkin, Weak decays of the B_c meson to charmonium and D mesons in the relativistic quark model, Phys. Rev. D **68**, 094020 (2003).

[20] C.-F. Qiao and R.-L. Zhu, Estimation of semileptonic decays of B_c meson to S-wave charmonia with nonrelativistic QCD, Phys. Rev. D **87**, 014009 (2013).

[21] C.-H. Chang, H.-F. Fu, G.-L. Wang, and J.-M. Zhang, Some of semileptonic and nonleptonic decays of B_c meson in a Bethe-Salpeter relativistic quark model, Sci. China Phys. Mech. Astron. **58**, 071001 (2015).

[22] M. A. Ivanov, J. G. Korner, and P. Santorelli, Exclusive semileptonic and nonleptonic decays of the B_c meson, Phys. Rev. D **73**, 054024 (2006).

[23] T. Huang and F. Zuo, Semileptonic B_c decays and charmonium distribution amplitude, Eur. Phys. J. C **51**, 833 (2007).

[24] W. Wang, Y.-L. Shen, and C.-D. Lu, Covariant light-front approach for B_c transition form factors, Phys. Rev. D **79**, 054012 (2009).

[25] E. Hernandez, J. Nieves, and J. M. Verde-Velasco, Study of exclusive semileptonic and non-leptonic decays of B_c^- in a nonrelativistic quark model, Phys. Rev. D **74**, 074008 (2006).

[26] P. Colangelo and F. De Fazio, Using heavy quark spin symmetry in semileptonic B_c decays, Phys. Rev. D **61**, 034012 (2000).

[27] I. P. Gouz, V. V. Kiselev, A. K. Likhoded, V. I. Romanovsky, and O. P. Yushchenko, Prospects for the B_c studies at LHCb, Phys. At. Nucl. **67**, 1559 (2004).

[28] A. Abd El-Hady, J. H. Munoz, and J. P. Vary, Semileptonic and nonleptonic B_c decays, Phys. Rev. D **62**, 014019 (2000).

[29] V. V. Kiselev, Exclusive decays and lifetime of B_c meson in QCD sum rules, arXiv:hep-ph/0211021.

[30] C.-H. Chang and Y.-Q. Chen, The decays of B_c meson, Phys. Rev. D **49**, 3399 (1994).

[31] M. A. Ivanov, J. G. Korner, and P. Santorelli, The semileptonic decays of the B_c meson, Phys. Rev. D **63**, 074010 (2001).

[32] D. Scora and N. Isgur, Semileptonic meson decays in the quark model: An update, Phys. Rev. D **52**, 2783 (1995).

[33] A. Yu. Anisimov, P. Yu. Kulikov, I. M. Narodetsky, and K. A. Ter-Martirosian, Exclusive and inclusive decays of the B_c meson in the light front ISGW model, Yad. Fiz. **62**, 1868 (1999) [Phys. At. Nucl. **62**, 1739 (1999)].

[34] D. Leljak, B. Melic, and M. Patra, On lepton flavour universality in semileptonic $B_c \to \eta_c$, J/ψ decays, J. High Energy Phys. 05 (2019) 094.

[35] A. A. Alves, Jr *et al.* (LHCb Collaboration), The LHCb detector at the LHC, J. Instrum. **3**, S08005 (2008).

[36] R. Aaij *et al.* (LHCb Collaboration), LHCb detector performance, Int. J. Mod. Phys. A **30**, 1530022 (2015).

[37] R. Aaij *et al.*, The LHCb trigger and its performance in 2011, J. Instrum. **8**, P04022 (2013).

[38] R. Aaij *et al.* (LHCb Collaboration), Measurement of b hadron production fractions in 7 TeV p p collisions, Phys. Rev. D **85**, 032008 (2012).

[39] V. V. Gligorov and M. Williams, Efficient, reliable and fast high-level triggering using a bonsai boosted decision tree, J. Instrum. **8**, P02013 (2013).

[40] T. Sjöstrand, S. Mrenna, and P. Skands, PYTHIA 6.4 physics and manual, J. High Energy Phys. 05 (2006) 026; A brief introduction to PYTHIA 8.1, Comput. Phys. Commun. **178**, 852 (2008).
[41] I. Belyaev *et al.*, Handling of the generation of primary events in Gauss, the LHCb simulation framework, J. Phys. Conf. Ser. **331**, 032047 (2011).
[42] D. J. Lange, The EvtGen particle decay simulation package, Nucl. Instrum. Methods Phys. Res., Sect. A **462**, 152 (2001).
[43] P. Golonka and Z. Was, PHOTOS Monte Carlo: A precision tool for QED corrections in Z and W decays, Eur. Phys. J. C **45**, 97 (2006).
[44] J. Allison *et al.* (Geant4 Collaboration), Geant4 developments and applications, IEEE Trans. Nucl. Sci. **53**, 270 (2006); S. Agostinelli *et al.* (Geant4 Collaboration), Geant4: A simulation toolkit, Nucl. Instrum. Methods Phys. Res., Sect. A **506**, 250 (2003).
[45] M. Clemencic, G. Corti, S. Easo, C. R Jones, S. Miglioranzi, M. Pappagallo, and P. Robbe, The LHCb simulation application, Gauss: Design, evolution and experience, J. Phys. Conf. Ser. **331**, 032023 (2011).
[46] H. Voss, A. Hoecker, J. Stelzer, and F. Tegenfeldt, TMVA—Toolkit for multivariate data analysis with ROOT, Proc. Sci., ACAT2007 (**2007**) 040; A. Hoecker *et al.*, TMVA 4—Toolkit for multivariate data analysis with ROOT. Users Guide, J. Instrum. **10**, P02007 (2015).
[47] R. Aaij *et al.* (LHCb Collaboration), Measurement of the ratio of branching fractions and difference in CP asymmetries of the decays $B^+ \to J/\psi\pi^+$ and $B^+ \to J/\psi K^+$, J. High Energy Phys. 03 (2017) 036.
[48] R. Aaij *et al.* (LHCb Collaboration), Measurement of the $B^\pm$ production asymmetry and the CP asymmetry in $B^\pm \to J/\psi K^\pm$ decays, Phys. Rev. D **95**, 052005 (2017).
[49] K. S. Cranmer, Kernel estimation in high-energy physics, Comput. Phys. Commun. **136**, 198 (2001).
[50] R. Aaij *et al.* (LHCb Collaboration), Measurement of the Ratio of Branching Fractions $\mathcal{B}(B_c^+ \to J/\psi\tau^+\nu_\tau)/\mathcal{B}(B_c^+ \to J/\psi\mu^+\nu_\mu)$, Phys. Rev. Lett. **120**, 121801 (2018).
[51] R. Aaij *et al.*, Selection and processing of calibration samples to measure the particle identification performance of the LHCb experiment in Run 2, Eur. Phys. J. Tech. Instrum. **6**, 1 (2018).
[52] R. Aaij *et al.* (LHCb Collaboration), Measurement of the track reconstruction efficiency at LHCb, J. Instrum. **10**, P02007 (2015).
[53] R. Aaij *et al.* (LHCb Collaboration), Measurement of the fragmentation fraction ratio f_s/f_d and its dependence on B meson kinematics, J. High Energy Phys. 04 (2013) 001.
[54] A. Ali, Q. Qin, and W. Wang, Discovery potential of stable and near-threshold doubly heavy tetraquarks at the LHC, Phys. Lett. B **785**, 605 (2018).

R. Aaij,[31] C. Abellán Beteta,[49] T. Ackernley,[59] B. Adeva,[45] M. Adinolfi,[53] H. Afsharnia,[9] C. A. Aidala,[79] S. Aiola,[25] Z. Ajaltouni,[9] S. Akar,[64] P. Albicocco,[22] J. Albrecht,[14] F. Alessio,[47] M. Alexander,[58] A. Alfonso Albero,[44] G. Alkhazov,[37] P. Alvarez Cartelle,[60] A. A. Alves Jr.,[45] S. Amato,[2] Y. Amhis,[11] L. An,[21] L. Anderlini,[21] G. Andreassi,[48] M. Andreotti,[20] F. Archilli,[16] J. Arnau Romeu,[10] A. Artamonov,[43] M. Artuso,[67] K. Arzymatov,[41] E. Aslanides,[10] M. Atzeni,[49] B. Audurier,[26] S. Bachmann,[16] J. J. Back,[55] S. Baker,[60] V. Balagura,[11,c] W. Baldini,[20,47] A. Baranov,[41] R. J. Barlow,[61] S. Barsuk,[11] W. Barter,[60] M. Bartolini,[23,47,i] F. Baryshnikov,[76] G. Bassi,[28] V. Batozskaya,[35] B. Batsukh,[67] A. Battig,[14] A. Bay,[48] M. Becker,[14] F. Bedeschi,[28] I. Bediaga,[1] A. Beiter,[67] L. J. Bel,[31] V. Belavin,[41] S. Belin,[26] N. Beliy,[5] V. Bellee,[48] K. Belous,[43] I. Belyaev,[38] G. Bencivenni,[22] E. Ben-Haim,[12] S. Benson,[31] S. Beranek,[13] A. Berezhnoy,[39] R. Bernet,[49] D. Berninghoff,[16] H. C. Bernstein,[67] E. Bertholet,[12] A. Bertolin,[27] C. Betancourt,[49] F. Betti,[19,f] M. O. Bettler,[54] Ia. Bezshyiko,[49] S. Bhasin,[53] J. Bhom,[33] M. S. Bieker,[14] S. Bifani,[52] P. Billoir,[12] A. Bizzeti,[21,v] M. Bjørn,[62] M. P. Blago,[47] T. Blake,[55] F. Blanc,[48] S. Blusk,[67] D. Bobulska,[58] V. Bocci,[30] O. Boente Garcia,[45] T. Boettcher,[63] A. Boldyrev,[77] A. Bondar,[42,y] N. Bondar,[37] S. Borghi,[61,47] M. Borisyak,[41] M. Borsato,[16] J. T. Borsuk,[33] T. J. V. Bowcock,[59] C. Bozzi,[20] M. J. Bradley,[60] S. Braun,[16] A. Brea Rodriguez,[45] M. Brodski,[47] J. Brodzicka,[33] A. Brossa Gonzalo,[55] D. Brundu,[26] E. Buchanan,[53] A. Buonaura,[49] C. Burr,[47] A. Bursche,[26] J. S. Butter,[31] J. Buytaert,[47] W. Byczynski,[47] S. Cadeddu,[26] H. Cai,[71] R. Calabrese,[20,h] L. Calero Diaz,[22] S. Cali,[22] R. Calladine,[52] M. Calvi,[24,j] M. Calvo Gomez,[44,n] A. Camboni,[44] P. Campana,[22] D. H. Campora Perez,[47] L. Capriotti,[19,f] A. Carbone,[19,f] G. Carboni,[29] R. Cardinale,[23,i] A. Cardini,[26] P. Carniti,[24,j] K. Carvalho Akiba,[31] A. Casais Vidal,[45] G. Casse,[59] M. Cattaneo,[47] G. Cavallero,[47] R. Cenci,[28,q] J. Cerasoli,[10] M. G. Chapman,[53] M. Charles,[12,47] Ph. Charpentier,[47] G. Chatzikonstantinidis,[52] M. Chefdeville,[8] V. Chekalina,[41] C. Chen,[3] S. Chen,[26] A. Chernov,[33] S.-G. Chitic,[47] V. Chobanova,[45] M. Chrzaszcz,[33] A. Chubykin,[37] P. Ciambrone,[22] M. F. Cicala,[55] X. Cid Vidal,[45] G. Ciezarek,[47] F. Cindolo,[19] P. E. L. Clarke,[57] M. Clemencic,[47] H. V. Cliff,[54] J. Closier,[47] J. L. Cobbledick,[61] V. Coco,[47] J. A. B. Coelho,[11] J. Cogan,[10] E. Cogneras,[9] L. Cojocariu,[36] P. Collins,[47] T. Colombo,[47] A. Comerma-Montells,[16] A. Contu,[26] N. Cooke,[52] G. Coombs,[58] S. Coquereau,[44] G. Corti,[47] C. M. Costa Sobral,[55] B. Couturier,[47] D. C. Craik,[63] J. Crkovska,[66] A. Crocombe,[55] M. Cruz Torres,[1] R. Currie,[57] C. L. Da Silva,[66] E. Dall'Occo,[14] J. Dalseno,[45,53] C. D'Ambrosio,[47] A. Danilina,[38] P. d'Argent,[16] A. Davis,[61] O. De Aguiar Francisco,[47] K. De Bruyn,[47] S. De Capua,[61]

M. De Cian,[48] J. M. De Miranda,[1] L. De Paula,[2] M. De Serio,[18,e] P. De Simone,[22] J. A. de Vries,[31] C. T. Dean,[66] W. Dean,[79] D. Decamp,[8] L. Del Buono,[12] B. Delaney,[54] H.-P. Dembinski,[15] M. Demmer,[14] A. Dendek,[34] V. Denysenko,[49] D. Derkach,[77] O. Deschamps,[9] F. Desse,[11] F. Dettori,[26] B. Dey,[7] A. Di Canto,[47] P. Di Nezza,[22] S. Didenko,[76] H. Dijkstra,[47] V. Dobishuk,[51] F. Dordei,[26] M. Dorigo,[28,z] A. C. dos Reis,[1] L. Douglas,[58] A. Dovbnya,[50] K. Dreimanis,[59] M. W. Dudek,[33] L. Dufour,[47] G. Dujany,[12] P. Durante,[47] J. M. Durham,[66] D. Dutta,[61] R. Dzhelyadin,[43,a] M. Dziewiecki,[16] A. Dziurda,[33] A. Dzyuba,[37] S. Easo,[56] U. Egede,[60] V. Egorychev,[38] S. Eidelman,[42,y] S. Eisenhardt,[57] R. Ekelhof,[14] S. Ek-In,[48] L. Eklund,[58] S. Ely,[67] A. Ene,[36] S. Escher,[13] S. Esen,[31] T. Evans,[47] A. Falabella,[19] J. Fan,[3] N. Farley,[52] S. Farry,[59] D. Fazzini,[11] M. Féo,[47] P. Fernandez Declara,[47] A. Fernandez Prieto,[45] F. Ferrari,[19,f] L. Ferreira Lopes,[48] F. Ferreira Rodrigues,[2] S. Ferreres Sole,[31] M. Ferrillo,[49] M. Ferro-Luzzi,[47] S. Filippov,[40] R. A. Fini,[18] M. Fiorini,[20,h] M. Firlej,[34] K. M. Fischer,[62] C. Fitzpatrick,[47] T. Fiutowski,[34] F. Fleuret,[11,c] M. Fontana,[47] F. Fontanelli,[23,i] R. Forty,[47] V. Franco Lima,[59] M. Franco Sevilla,[65] M. Frank,[47] C. Frei,[47] D. A. Friday,[58] J. Fu,[25,r] M. Fuehring,[14] W. Funk,[47] E. Gabriel,[57] A. Gallas Torreira,[45] D. Galli,[19,f] S. Gallorini,[27] S. Gambetta,[57] Y. Gan,[3] M. Gandelman,[2] P. Gandini,[25] Y. Gao,[4] L. M. Garcia Martin,[46] J. García Pardiñas,[49] B. Garcia Plana,[45] F. A. Garcia Rosales,[11] J. Garra Tico,[54] L. Garrido,[44] D. Gascon,[44] C. Gaspar,[47] D. Gerick,[16] E. Gersabeck,[61] M. Gersabeck,[61] T. Gershon,[55] D. Gerstel,[10] Ph. Ghez,[8] V. Gibson,[54] A. Gioventù,[45] O. G. Girard,[48] P. Gironella Gironell,[44] L. Giubega,[36] C. Giugliano,[20] K. Gizdov,[57] V. V. Gligorov,[12] C. Göbel,[69] D. Golubkov,[38] A. Golutvin,[60,76] A. Gomes,[1,b] P. Gorbounov,[38,6] I. V. Gorelov,[39] C. Gotti,[24,j] E. Govorkova,[31] J. P. Grabowski,[16] R. Graciani Diaz,[44] T. Grammatico,[12] L. A. Granado Cardoso,[47] E. Graugés,[44] E. Graverini,[48] G. Graziani,[21] A. Grecu,[36] R. Greim,[31] P. Griffith,[20] L. Grillo,[61] L. Gruber,[47] B. R. Gruberg Cazon,[62] C. Gu,[3] E. Gushchin,[40] A. Guth,[13] Yu. Guz,[43,47] T. Gys,[47] T. Hadavizadeh,[62] G. Haefeli,[48] C. Haen,[47] S. C. Haines,[54] P. M. Hamilton,[65] Q. Han,[7] X. Han,[16] T. H. Hancock,[62] S. Hansmann-Menzemer,[16] N. Harnew,[62] T. Harrison,[59] R. Hart,[31] C. Hasse,[47] M. Hatch,[47] J. He,[5] M. Hecker,[60] K. Heijhoff,[31] K. Heinicke,[14] A. Heister,[14] A. M. Hennequin,[47] K. Hennessy,[59] L. Henry,[46] J. Heuel,[13] A. Hicheur,[68] R. Hidalgo Charman,[61] D. Hill,[62] M. Hilton,[61] P. H. Hopchev,[48] J. Hu,[16] W. Hu,[7] W. Huang,[5] W. Hulsbergen,[31] T. Humair,[60] R. J. Hunter,[55] M. Hushchyn,[77] D. Hutchcroft,[59] D. Hynds,[31] P. Ibis,[14] M. Idzik,[34] P. Ilten,[52] A. Inglessi,[37] A. Inyakin,[43] K. Ivshin,[37] R. Jacobsson,[47] S. Jakobsen,[47] J. Jalocha,[62] E. Jans,[31] B. K. Jashal,[46] A. Jawahery,[65] V. Jevtic,[14] F. Jiang,[3] M. John,[62] D. Johnson,[47] C. R. Jones,[54] B. Jost,[47] N. Jurik,[62] S. Kandybei,[50] M. Karacson,[47] J. M. Kariuki,[53] N. Kazeev,[77] M. Kecke,[16] F. Keizer,[54,54] M. Kelsey,[67] M. Kenzie,[54] T. Ketel,[32] B. Khanji,[47] A. Kharisova,[78] K. E. Kim,[67] T. Kirn,[13] V. S. Kirsebom,[48] S. Klaver,[22] K. Klimaszewski,[35] S. Koliiev,[51] A. Kondybayeva,[76] A. Konoplyannikov,[38] P. Kopciewicz,[34] R. Kopecna,[16] P. Koppenburg,[31] I. Kostiuk,[31,51] O. Kot,[51] S. Kotriakhova,[37] L. Kravchuk,[40] R. D. Krawczyk,[47] M. Kreps,[55] F. Kress,[60] S. Kretzschmar,[13] P. Krokovny,[42,y] W. Krupa,[34] W. Krzemien,[35] W. Kucewicz,[33,m] M. Kucharczyk,[33] V. Kudryavtsev,[42,y] H. S. Kuindersma,[31] G. J. Kunde,[66] T. Kvaratskheliya,[38] D. Lacarrere,[47] G. Lafferty,[61] A. Lai,[26] D. Lancierini,[49] J. J. Lane,[61] G. Lanfranchi,[22] C. Langenbruch,[13] T. Latham,[55] F. Lazzari,[28,w] C. Lazzeroni,[52] R. Le Gac,[10] R. Lefèvre,[9] A. Leflat,[39] F. Lemaitre,[47] O. Leroy,[10] T. Lesiak,[33] B. Leverington,[16] H. Li,[70] X. Li,[66] Y. Li,[6] Z. Li,[67] X. Liang,[67] R. Lindner,[47] V. Lisovskyi,[11] G. Liu,[70] X. Liu,[3] D. Loh,[55] A. Loi,[26] J. Lomba Castro,[45] I. Longstaff,[58] J. H. Lopes,[2] G. Loustau,[49] G. H. Lovell,[54] Y. Lu,[6] D. Lucchesi,[27,p] M. Lucio Martinez,[31] Y. Luo,[3] A. Lupato,[27] E. Luppi,[20,h] O. Lupton,[55] A. Lusiani,[28] X. Lyu,[5] S. Maccolini,[19,f] F. Machefert,[11] F. Maciuc,[36] V. Macko,[48] P. Mackowiak,[14] S. Maddrell-Mander,[53] L. R. Madhan Mohan,[53] O. Maev,[37,47] A. Maevskiy,[77] D. Maisuzenko,[37] M. W. Majewski,[34] S. Malde,[62] B. Malecki,[47] A. Malinin,[75] T. Maltsev,[42,y] H. Malygina,[16] G. Manca,[26,g] G. Mancinelli,[10] R. Manera Escalero,[44] D. Manuzzi,[19,f] D. Marangotto,[25,r] J. Maratas,[9,x] J. F. Marchand,[8] U. Marconi,[19] S. Mariani,[21] C. Marin Benito,[11] M. Marinangeli,[48] P. Marino,[48] J. Marks,[16] P. J. Marshall,[59] G. Martellotti,[30] L. Martinazzoli,[47] M. Martinelli,[24] D. Martinez Santos,[45] F. Martinez Vidal,[46] A. Massafferri,[1] M. Materok,[13] R. Matev,[47] A. Mathad,[49] Z. Mathe,[47] V. Matiunin,[38] C. Matteuzzi,[24] K. R. Mattioli,[79] A. Mauri,[49] E. Maurice,[11,c] M. McCann,[60,47] L. Mcconnell,[17] A. McNab,[61] R. McNulty,[17] J. V. Mead,[59] B. Meadows,[64] C. Meaux,[10] G. Meier,[14] N. Meinert,[73] D. Melnychuk,[35] S. Meloni,[24,j] M. Merk,[31] A. Merli,[25] M. Mikhasenko,[47] D. A. Milanes,[72] E. Millard,[55] M.-N. Minard,[8] O. Mineev,[38] L. Minzoni,[20,h] S. E. Mitchell,[57] B. Mitreska,[61] D. S. Mitzel,[47] A. Mödden,[14] A. Mogini,[12] R. D. Moise,[60] T. Mombächer,[14] I. A. Monroy,[72] S. Monteil,[9] M. Morandin,[27] G. Morello,[22] M. J. Morello,[28,u] J. Moron,[34] A. B. Morris,[10] A. G. Morris,[55] R. Mountain,[67] H. Mu,[3] F. Muheim,[57] M. Mukherjee,[7] M. Mulder,[31] D. Müller,[47] K. Müller,[49] V. Müller,[14] C. H. Murphy,[62] D. Murray,[61] P. Muzzetto,[26] P. Naik,[53] T. Nakada,[48] R. Nandakumar,[56] A. Nandi,[62] T. Nanut,[48] I. Nasteva,[2] M. Needham,[57] N. Neri,[25,r] S. Neubert,[16] N. Neufeld,[47] R. Newcombe,[60] T. D. Nguyen,[48] C. Nguyen-Mau,[48,o] E. M. Niel,[11] S. Nieswand,[13] N. Nikitin,[39] N. S. Nolte,[47] C. Nunez,[79] A. Oblakowska-Mucha,[34] V. Obraztsov,[43] S. Ogilvy,[58] D. P. O'Hanlon,[19] R. Oldeman,[26,g]

C. J. G. Onderwater,[74] J. D. Osborn,[79] A. Ossowska,[33] J. M. Otalora Goicochea,[2] T. Ovsiannikova,[38] P. Owen,[49] A. Oyanguren,[46] P. R. Pais,[48] T. Pajero,[28,u] A. Palano,[18] M. Palutan,[22] G. Panshin,[78] A. Papanestis,[56] M. Pappagallo,[57] L. L. Pappalardo,[20,h] C. Pappenheimer,[64] W. Parker,[65] C. Parkes,[61] G. Passaleva,[21,47] A. Pastore,[18] M. Patel,[60] C. Patrignani,[19,f] A. Pearce,[47] A. Pellegrino,[31] M. Pepe Altarelli,[47] S. Perazzini,[19] D. Pereima,[38] P. Perret,[9] L. Pescatore,[48] K. Petridis,[53] A. Petrolini,[23,i] A. Petrov,[75] S. Petrucci,[57] M. Petruzzo,[25,r] B. Pietrzyk,[8] G. Pietrzyk,[48] M. Pikies,[33] M. Pili,[62] D. Pinci,[30] J. Pinzino,[47] F. Pisani,[47] A. Piucci,[16] V. Placinta,[36] S. Playfer,[57] J. Plews,[52] M. Plo Casasus,[45] F. Polci,[12] M. Poli Lener,[22] M. Poliakova,[67] A. Poluektov,[10] N. Polukhina,[76,d] I. Polyakov,[67] E. Polycarpo,[2] G. J. Pomery,[53] S. Ponce,[47] A. Popov,[43] D. Popov,[52] S. Poslavskii,[43] K. Prasanth,[33] L. Promberger,[47] C. Prouve,[45] V. Pugatch,[51] A. Puig Navarro,[49] H. Pullen,[62] G. Punzi,[28,q] W. Qian,[5] J. Qin,[5] R. Quagliani,[12] B. Quintana,[9] N. V. Raab,[17] R. I. Rabadan Trejo,[10] B. Rachwal,[34] J. H. Rademacker,[53] M. Rama,[28] M. Ramos Pernas,[45] M. S. Rangel,[2] F. Ratnikov,[41,77] G. Raven,[32] M. Reboud,[8] F. Redi,[48] F. Reiss,[12] C. Remon Alepuz,[46] Z. Ren,[3] V. Renaudin,[62] S. Ricciardi,[56] S. Richards,[53] K. Rinnert,[59] P. Robbe,[11] A. Robert,[12] A. B. Rodrigues,[48] E. Rodrigues,[64] J. A. Rodriguez Lopez,[72] M. Roehrken,[47] S. Roiser,[47] A. Rollings,[62] V. Romanovskiy,[43] M. Romero Lamas,[45] A. Romero Vidal,[45] J. D. Roth,[79] M. Rotondo,[22] M. S. Rudolph,[67] T. Ruf,[47] J. Ruiz Vidal,[46] J. Ryzka,[34] J. J. Saborido Silva,[45] N. Sagidova,[37] B. Saitta,[26,g] C. Sanchez Gras,[31] C. Sanchez Mayordomo,[46] B. Sanmartin Sedes,[45] R. Santacesaria,[30] C. Santamarina Rios,[45] M. Santimaria,[22] E. Santovetti,[29,k] G. Sarpis,[61] A. Sarti,[30] C. Satriano,[30,t] A. Satta,[29] M. Saur,[5] D. Savrina,[38,39] L. G. Scantlebury Smead,[62] S. Schael,[13] M. Schellenberg,[14] M. Schiller,[58] H. Schindler,[47] M. Schmelling,[15] T. Schmelzer,[14] B. Schmidt,[47] O. Schneider,[48] A. Schopper,[47] H. F. Schreiner,[64] M. Schubiger,[31] S. Schulte,[48] M. H. Schune,[11] R. Schwemmer,[47] B. Sciascia,[22] A. Sciubba,[30,l] S. Sellam,[68] A. Semennikov,[38] A. Sergi,[52,47] N. Serra,[49] J. Serrano,[10] L. Sestini,[27] A. Seuthe,[14] P. Seyfert,[47] D. M. Shangase,[79] M. Shapkin,[43] T. Shears,[59] L. Shekhtman,[42,y] V. Shevchenko,[75,76] E. Shmanin,[76] J. D. Shupperd,[67] B. G. Siddi,[20] R. Silva Coutinho,[49] L. Silva de Oliveira,[2] G. Simi,[27,p] S. Simone,[18,e] I. Skiba,[20] N. Skidmore,[16] T. Skwarnicki,[67] M. W. Slater,[52] J. G. Smeaton,[54] A. Smetkina,[38] E. Smith,[13] I. T. Smith,[57] M. Smith,[60] A. Snoch,[31] M. Soares,[19] L. Soares Lavra,[1] M. D. Sokoloff,[64] F. J. P. Soler,[58] B. Souza De Paula,[2] B. Spaan,[14] E. Spadaro Norella,[25,r] P. Spradlin,[58] F. Stagni,[47] M. Stahl,[64] S. Stahl,[47] P. Stefko,[48] S. Stefkova,[60] O. Steinkamp,[49] S. Stemmle,[16] O. Stenyakin,[43] M. Stepanova,[37] H. Stevens,[14] S. Stone,[67] S. Stracka,[28] M. E. Stramaglia,[48] M. Straticiuc,[36] S. Strokov,[78] J. Sun,[3] L. Sun,[71] Y. Sun,[65] P. Svihra,[61] K. Swientek,[34] A. Szabelski,[35] T. Szumlak,[34] M. Szymanski,[5] S. Taneja,[61] Z. Tang,[3] T. Tekampe,[14] G. Tellarini,[20] F. Teubert,[47] E. Thomas,[47] K. A. Thomson,[59] M. J. Tilley,[60] V. Tisserand,[9] S. T'Jampens,[8] M. Tobin,[6] S. Tolk,[47] L. Tomassetti,[20,h] D. Tonelli,[28] D. Y. Tou,[12] E. Tournefier,[8] M. Traill,[58] M. T. Tran,[48] C. Trippl,[48] A. Trisovic,[54] A. Tsaregorodtsev,[10] G. Tuci,[28,47,q] A. Tully,[48] N. Tuning,[31] A. Ukleja,[35] A. Usachov,[11] A. Ustyuzhanin,[41,77] U. Uwer,[16] A. Vagner,[78] V. Vagnoni,[19] A. Valassi,[47] G. Valenti,[19] M. van Beuzekom,[31] H. Van Hecke,[66] E. van Herwijnen,[47] C. B. Van Hulse,[17] M. van Veghel,[74] R. Vazquez Gomez,[44] P. Vazquez Regueiro,[45] C. Vázquez Sierra,[31] S. Vecchi,[20] J. J. Velthuis,[53] M. Veltri,[21,s] A. Venkateswaran,[67] M. Vernet,[9] M. Veronesi,[31] M. Vesterinen,[55] J. V. Viana Barbosa,[47] D. Vieira,[5] M. Vieites Diaz,[48] H. Viemann,[73] X. Vilasis-Cardona,[44,n] A. Vitkovskiy,[31] V. Volkov,[39] A. Vollhardt,[49] D. Vom Bruch,[12] A. Vorobyev,[37] V. Vorobyev,[42,y] N. Voropaev,[37] R. Waldi,[73] J. Walsh,[28] J. Wang,[3] J. Wang,[71] J. Wang,[6] M. Wang,[3] Y. Wang,[7] Z. Wang,[49] D. R. Ward,[54] H. M. Wark,[59] N. K. Watson,[52] D. Websdale,[60] A. Weiden,[49] C. Weisser,[63] B. D. C. Westhenry,[53] D. J. White,[61] M. Whitehead,[13] D. Wiedner,[14] G. Wilkinson,[62] M. Wilkinson,[67] I. Williams,[54] M. Williams,[63] M. R. J. Williams,[61] T. Williams,[52] F. F. Wilson,[56] M. Winn,[11] W. Wislicki,[35] M. Witek,[33] G. Wormser,[11] S. A. Wotton,[54] H. Wu,[67] K. Wyllie,[47] Z. Xiang,[5] D. Xiao,[7] Y. Xie,[7] H. Xing,[70] A. Xu,[3] L. Xu,[3] M. Xu,[7] Q. Xu,[5] Z. Xu,[8] Z. Xu,[3] Z. Yang,[3] Z. Yang,[65] Y. Yao,[67] L. E. Yeomans,[59] H. Yin,[7] J. Yu,[7,ab] X. Yuan,[67] O. Yushchenko,[43] K. A. Zarebski,[52] M. Zavertyaev,[15,d] M. Zdybal,[33] M. Zeng,[3] D. Zhang,[7] L. Zhang,[3] S. Zhang,[3] W. C. Zhang,[3,aa] Y. Zhang,[47] A. Zhelezov,[16] Y. Zheng,[5] X. Zhou,[5] Y. Zhou,[5] X. Zhu,[3] V. Zhukov,[13,39] J. B. Zonneveld,[57] and S. Zucchelli[19,f]

(LHCb Collaboration)

[1]*Centro Brasileiro de Pesquisas Físicas (CBPF), Rio de Janeiro, Brazil*
[2]*Universidade Federal do Rio de Janeiro (UFRJ), Rio de Janeiro, Brazil*
[3]*Center for High Energy Physics, Tsinghua University, Beijing, China*
[4]*School of Physics State Key Laboratory of Nuclear Physics and Technology, Peking University, Beijing, China*
[5]*University of Chinese Academy of Sciences, Beijing, China*

[6]*Institute Of High Energy Physics (IHEP), Beijing, China*
[7]*Institute of Particle Physics, Central China Normal University, Wuhan, Hubei, China*
[8]*Univ. Grenoble Alpes, Univ. Savoie Mont Blanc, CNRS, IN2P3-LAPP, Annecy, France*
[9]*Université Clermont Auvergne, CNRS/IN2P3, LPC, Clermont-Ferrand, France*
[10]*Aix Marseille Univ, CNRS/IN2P3, CPPM, Marseille, France*
[11]*LAL, Univ. Paris-Sud, CNRS/IN2P3, Université Paris-Saclay, Orsay, France*
[12]*LPNHE, Sorbonne Université, Paris Diderot Sorbonne Paris Cité, CNRS/IN2P3, Paris, France*
[13]*I. Physikalisches Institut, RWTH Aachen University, Aachen, Germany*
[14]*Fakultät Physik, Technische Universität Dortmund, Dortmund, Germany*
[15]*Max-Planck-Institut für Kernphysik (MPIK), Heidelberg, Germany*
[16]*Physikalisches Institut, Ruprecht-Karls-Universität Heidelberg, Heidelberg, Germany*
[17]*School of Physics, University College Dublin, Dublin, Ireland*
[18]*INFN Sezione di Bari, Bari, Italy*
[19]*INFN Sezione di Bologna, Bologna, Italy*
[20]*INFN Sezione di Ferrara, Ferrara, Italy*
[21]*INFN Sezione di Firenze, Firenze, Italy*
[22]*INFN Laboratori Nazionali di Frascati, Frascati, Italy*
[23]*INFN Sezione di Genova, Genova, Italy*
[24]*INFN Sezione di Milano-Bicocca, Milano, Italy*
[25]*INFN Sezione di Milano, Milano, Italy*
[26]*INFN Sezione di Cagliari, Monserrato, Italy*
[27]*INFN Sezione di Padova, Padova, Italy*
[28]*INFN Sezione di Pisa, Pisa, Italy*
[29]*INFN Sezione di Roma Tor Vergata, Roma, Italy*
[30]*INFN Sezione di Roma La Sapienza, Roma, Italy*
[31]*Nikhef National Institute for Subatomic Physics, Amsterdam, Netherlands*
[32]*Nikhef National Institute for Subatomic Physics and VU University Amsterdam, Amsterdam, Netherlands*
[33]*Henryk Niewodniczanski Institute of Nuclear Physics Polish Academy of Sciences, Kraków, Poland*
[34]*AGH—University of Science and Technology, Faculty of Physics and Applied Computer Science, Kraków, Poland*
[35]*National Center for Nuclear Research (NCBJ), Warsaw, Poland*
[36]*Horia Hulubei National Institute of Physics and Nuclear Engineering, Bucharest-Magurele, Romania*
[37]*Petersburg Nuclear Physics Institute NRC Kurchatov Institute (PNPI NRC KI), Gatchina, Russia*
[38]*Institute of Theoretical and Experimental Physics NRC Kurchatov Institute (ITEP NRC KI), Moscow, Russia, Moscow, Russia*
[39]*Institute of Nuclear Physics, Moscow State University (SINP MSU), Moscow, Russia*
[40]*Institute for Nuclear Research of the Russian Academy of Sciences (INR RAS), Moscow, Russia*
[41]*Yandex School of Data Analysis, Moscow, Russia*
[42]*Budker Institute of Nuclear Physics (SB RAS), Novosibirsk, Russia*
[43]*Institute for High Energy Physics NRC Kurchatov Institute (IHEP NRC KI), Protvino, Russia, Protvino, Russia*
[44]*ICCUB, Universitat de Barcelona, Barcelona, Spain*
[45]*Instituto Galego de Física de Altas Enerxías (IGFAE), Universidade de Santiago de Compostela, Santiago de Compostela, Spain*
[46]*Instituto de Fisica Corpuscular, Centro Mixto Universidad de Valencia—CSIC, Valencia, Spain*
[47]*European Organization for Nuclear Research (CERN), Geneva, Switzerland*
[48]*Institute of Physics, Ecole Polytechnique Fédérale de Lausanne (EPFL), Lausanne, Switzerland*
[49]*Physik-Institut, Universität Zürich, Zürich, Switzerland*
[50]*NSC Kharkiv Institute of Physics and Technology (NSC KIPT), Kharkiv, Ukraine*
[51]*Institute for Nuclear Research of the National Academy of Sciences (KINR), Kyiv, Ukraine*
[52]*University of Birmingham, Birmingham, United Kingdom*
[53]*H.H. Wills Physics Laboratory, University of Bristol, Bristol, United Kingdom*
[54]*Cavendish Laboratory, University of Cambridge, Cambridge, United Kingdom*
[55]*Department of Physics, University of Warwick, Coventry, United Kingdom*
[56]*STFC Rutherford Appleton Laboratory, Didcot, United Kingdom*
[57]*School of Physics and Astronomy, University of Edinburgh, Edinburgh, United Kingdom*
[58]*School of Physics and Astronomy, University of Glasgow, Glasgow, United Kingdom*
[59]*Oliver Lodge Laboratory, University of Liverpool, Liverpool, United Kingdom*
[60]*Imperial College London, London, United Kingdom*
[61]*Department of Physics and Astronomy, University of Manchester, Manchester, United Kingdom*

[62]Department of Physics, University of Oxford, Oxford, United Kingdom
[63]Massachusetts Institute of Technology, Cambridge, Massachusetts, USA
[64]University of Cincinnati, Cincinnati, Ohio, USA
[65]University of Maryland, College Park, Maryland, USA
[66]Los Alamos National Laboratory (LANL), Los Alamos, New Mexico, USA
[67]Syracuse University, Syracuse, New York, USA
[68]Laboratory of Mathematical and Subatomic Physics, Constantine, Algeria
[associated with Universidade Federal do Rio de Janeiro (UFRJ)]
[69]Pontifícia Universidade Católica do Rio de Janeiro (PUC-Rio), Rio de Janeiro, Brazil
[associated with Universidade Federal do Rio de Janeiro (UFRJ)]
[70]South China Normal University, Guangzhou, China, associated with Center for High Energy Physics
[71]School of Physics and Technology, Wuhan University, Wuhan, China
(associated with Center for High Energy Physics)
[72]Departamento de Fisica, Universidad Nacional de Colombia, Bogota, Colombia
(associated with LPNHE)
[73]Institut für Physik, Universität Rostock, Rostock, Germany (associated with Physikalisches Institut)
[74]Van Swinderen Institute, University of Groningen, Groningen, Netherlands
(associated with Nikhef National Institute for Subatomic Physics)
[75]National Research Centre Kurchatov Institute, Moscow, Russia [associated with Institute of Theoretical and Experimental Physics NRC Kurchatov Institute (ITEP NRC KI)]
[76]National University of Science and Technology "MISIS," Moscow, Russia [associated with Institute of Theoretical and Experimental Physics NRC Kurchatov Institute (ITEP NRC KI)]
[77]National Research University Higher School of Economics, Moscow, Russia
(associated with Yandex School of Data Analysis)
[78]National Research Tomsk Polytechnic University, Tomsk, Russia
[associated with Institute of Theoretical and Experimental Physics NRC Kurchatov Institute (ITEP NRC KI)]
[79]University of Michigan, Ann Arbor, USA (associated with Syracuse University)

[a]Deceased.
[b]Also at Universidade Federal do Triângulo Mineiro (UFTM), Uberaba-MG, Brazil.
[c]Also at Laboratoire Leprince-Ringuet, Palaiseau, France.
[d]Also at P.N. Lebedev Physical Institute, Russian Academy of Science (LPI RAS), Moscow, Russia.
[e]Also at Università di Bari, Bari, Italy.
[f]Also at Università di Bologna, Bologna, Italy.
[g]Also at Università di Cagliari, Cagliari, Italy.
[h]Also at Università di Ferrara, Ferrara, Italy.
[i]Also at Università di Genova, Genova, Italy.
[j]Also at Università di Milano Bicocca, Milano, Italy.
[k]Also at Università di Roma Tor Vergata, Roma, Italy.
[l]Also at Università di Roma La Sapienza, Roma, Italy.
[m]Also at AGH—University of Science and Technology, Faculty of Computer Science, Electronics and Telecommunications, Kraków, Poland.
[n]Also at LIFAELS, La Salle, Universitat Ramon Llull, Barcelona, Spain.
[o]Also at Hanoi University of Science, Hanoi, Vietnam.
[p]Also at Università di Padova, Padova, Italy.
[q]Also at Università di Pisa, Pisa, Italy.
[r]Also at Università degli Studi di Milano, Milano, Italy.
[s]Also at Università di Urbino, Urbino, Italy.
[t]Also at Università della Basilicata, Potenza, Italy.
[u]Also at Scuola Normale Superiore, Pisa, Italy.
[v]Also at Università di Modena e Reggio Emilia, Modena, Italy.
[w]Also at Università di Siena, Siena, Italy.
[x]Also at MSU—Iligan Institute of Technology (MSU-IIT), Iligan, Philippines.
[y]Also at Novosibirsk State University, Novosibirsk, Russia.
[z]Also at INFN Sezione di Trieste, Trieste, Italy.
[aa]Also at School of Physics and Information Technology, Shaanxi Normal University (SNNU), Xi'an, China.
[ab]Also at Physics and Micro Electronic College, Hunan University, Changsha City, China.